TAMPEREEN TEKNILLINEN YLIOPISTO
TAMPERE UNIVERSITY OF TECHNOLOGY

MARKEL ARIZABALETA

OPTIMIZATION CRITERIA FOR JOINT COMMUNICATION AND POSITIONING NETWORKS

Master of Science Thesis

Examiners: Assoc. prof. Elena-Simona Lohan and Dr. Jukka Talvitie
Examiners and topic approved on 16 January 2017

ABSTRACT

FIRSTNAME LASTNAME: Markel Arizabaleta
Tampere University of technology
Master of Science Thesis, 77 pages, 0 Appendix pages
May 2017
Master's Degree Programme in Information Technology
Major: Communication systems and Networking
Examiners: Assoc. Prof. Elena-Simona Lohan and Dr. Jukka Talvitie

Keywords: 5G, communication, positioning, Cramer Rao Lower Bound (CRLB), mmWave, Received Signal Strength (RSS)

The current mobile system, namely 4G, has limitations in applications where low latency and high data rates are needed. In addition, new applications require a very precise user positioning, which 4G is not able to provide with high availability. In order to face these problems, a new mobile system is being developed, namely 5G. The 5G system is likely to be designed as a joint communication and positioning system. This thesis focuses on couple of performance criteria in the context of 5G systems, namely the accuracy of the estimation of time-delay, which is directly proportional to the positioning accuracy, and the Quality of Service (QoS) of the communications, measured here in terms of the Bit Error Rates (BER). Our studies are based on three different waveforms proposed in the context of future 5G and mmWave frequencies (3-300GHz). The analysis is performed in two different scenarios, outdoor and indoor, and with different modulation orders. For each scenario, a channel model has been developed. The outdoor channel model is based on the channel model created for the 5G system in the European METIS project. For the indoor scenarios, the indoor maps of one multi-floor building in Tampere University of Technology are used. The results show that the modulation order has no influence on the positioning accuracy, but it is very important in the communication QoS. In addition, minor differences are observed from the selected three waveforms in terms of the joint positioning and communication performance, in such a way that there is no clear advantage in terms of positioning accuracy of one waveform over the other, among the three considered cases. The performance difference is higher at the communication side, where a difference of 1dB between the waveforms is obtained to achieve the same BER value, the best being CP-OFDM.

PREFACE

This thesis is carried out during the 2016/2017 academic year at the Department of Electronics and Communications Engineering, Tampere University of Technology, Tampere, Finland.

I would like to express my deepest gratitude to my supervisors Assoc. Prof. Elena-Simona Lohan and Dr. Jukka Talvitie, for their guidance during this year. Their support has motivated me to work, especially- in hard times.

I also wish to dedicate special thanks to my parents Juan Ramón and Indalecia, as well as my sister Naiara for their help and support in my studies during all this year. Most of all, I want to thank my aunt Isabel, my uncle Juan Manuel, and my grandparents Ovidio and Mari Iluminada. Thank you all.

Tampere, May 2017

Markel Arizabaleta

CONTENTS

LIST OF FIGURES

LIST OF TABLES

LIST OF ABBREVIATIONS

A-GPS	Assisted Global Positioning System
AMPS	Advance Mobile Phone System
AOA	Angel of Arrival
BER	Bit Error Rate
BS	Base Station
BW	Bandwidth
CERP	Circular Error Probability
CGI	Cell Global Identity
COQAM	Circular Offset Quadrature Amplitude Multiplexing
CP	Cyclic-prefix
CP-OFDMA	Cyclic-prefix Orthogonal Frequency Division Multiple Access
CRLB	Cramer Rao Lower Bound
DFT	Discrete Fourier Transform
DFT-s-OFDMA	Discrete Fourier Transform spread Orthogonal Frequency Division Multiple Access
E-OTD	Enhanced Observed Time Difference
E2E	End-to-end
EDGE	Enhanced Data rate for GSM Evolution
EKF	Extended Kalman Filter
EPA	Extended Pedestrian A
ETU	Extended Typical Urban
EVA	Extended Vehicular A
FBMC	Filter Bank Multi-Carrier
FIM	Fisher Information Matrix
FFT	Fast Fourier Transform
FMT	Filtered Multitone
F-OFDM	Filtered Orthogonal Frequency Division Multiplexing
GFDM	Generalized Frequency Domain Multiplexing
GMSK	Gaussian Minimum Shift Keying
GPS	Global Positioning System
GSM	Global System for Mobile communications
GUI	Graphical User Interface
HSPA	High-Speed Packet Access
HSPA+	Evolved High-Speed Packet Access
IPDL	Idle Period on the Downlink
JML	Joint Maximum Likelihood
KPI	Key Performance Indicator
IFFT	Inverse Fast Fourier Transform
IoT	Internet of Things
LOS	Line of Sight
LTE	Long Term Evolution
M2M	Machine-to-machine
MAC	Medium Access Control
MCL	Minimum Coupling Loss
METIS	Mobile and Wireless Communications Enablers for the Twenty-Twenty Information Society
MIMO	Multiple Input-Multiple Output
MINT	Multipath-assisted Indoor Navigation and Tracking
mmWaves	Millimeter Waves
MT	Mobile Terminal
MUSIC	Multiple Signal Classification

NLOS	Non-Line of Sight
NMT	Nordic Mobile Terminal
NSE	Network Spectral Efficiency
OFDM	Orthogonal Frequency Division Multiplexing
OQAM	Offset Quadrature Amplitude Multiplexing
OTDOA	Observed Time Difference of Arrival
OTT	One-Trip time latency
PDF	Power-Spectral Density Function
PER	Packet Error Rate
PHY	Physical layer
PRS	Positioning Reference Signal
QAM	Quadrature Amplitude Modulation
QoE	Quality of Experience
QoS	Quality of Service
RAN	Radio Access Network
RMS	Root mean square
RMSE	Root mean square Error
RSS	Received Signal Strength
RTT	Round-Trip time latency
SER	Symbol Error Rate
SERP	Spherical Error Probability
SINR	Signal to Interference plus Noise Ratio
SNR	Signal to Noise Ratio
SRRC	Square Root Rise Cosine
STAMP	Simultaneous Target And Multipath Positioning
TA	Timing Advance
TACS	Total Access Communication System
TDMA	Time Division Multiple Access
TUT	Tampere University of Technology
U-TDOA	Uplink Time Difference of Arrival
UF-OFDM	Universal Filtered Orthogonal Frequency Division Multiplexing
UFMC	Universal Filterec Multicarrier
UHD	Ultra-High Definition
UL-TOA	Uplink Time of Arrival
UMTS	Universal Mobile Telecommunication Service
UPLS	User Plan Location Support
WCP-COQAM	Wideband Cyclic-Prefix Cyclic Offset Quadrature Amplitude Modulation
W-OFDM	Windowing Orthogonal Frequency Division Multiplex
WINNER	Wireless world Initiative New Radio
ZT-DFT-s-OFDMA	Zero Tail Discrete Fourier Transform spread Orthogonal Frequency Division Multiple Access

LIST OF SYMBOLS

T_x	Transmitted signal power
L_{LS}	Attenuation added by long-scale propagation effects
L_{MS}	Attenuation added by medium-scale propagation effects
L_{SS}	Attenuation added by small-scale propagation effects
d	Distance between transmitter and receiver
λ	Wavelength
T_0	Signal Transmission Time
T_i	Signal Reception Time
c	Speed of Light
ε_b	Distance error caused by the clock bias
$\Delta T_{i,j}$	Propagation delay difference
$\Delta d_{i,j}$	Distance difference
n_i	TOA measurement errors between the i-th BS and MT
x	Position of the user in the X axis
y_t	Position of the user in the Y axis
$L_{i,k}$	Length of the packet k of the user i in bits
$T_{i,k}$	End-to-end delay of the packet k and the i-th user in seconds
$R_{i,k}$	Throughput of the packet k and the i-th user in packets/seconds
Th_i	End-user throughput of the i-th user
Wdata	Available bandwidth
𝟙align	Indicator function of beam alignment
PRX	Power of the receiving signal
PAWGN	Power of the
Eeff	Energy efficiency
λI	Energy per information bit
E	Consumed energy
I	Information volume
R	Information rate
P	Consumed Power
λA	Power per area unit
A	Covered area
$\hat{x}_k$	Estimated user position in the X axis
$\hat{y}_k$	Estimated user position in the Y axis
$\hat{z}_k$	Estimated user position in the Z axis
σ^2_{CRLB}	CRLB variance
β2	Equivalent bandwidth
S(f)	Signal spectrum
σ_φ	Standard deviation of the DOA estimation error
τ	Delay samples
t_ϵ	Propagation delay
Ts	Sampling time
M	Number of subcarriers
c_m	Complex valued data symbols
MIFFT	Number of points in the IFFT operation
Mt	Number of zero valued symbols added in the tail
Mh	Number of zero valued symbols added in the head
g	Prototype filter
N1	Discrete time offset
$\Phi_{m,n}$	Additional phase term at subcarrier m and symbol n
K’	Number of real symbol slots per block

LCP	Length of the cyclic prefix
$\hat{\tau}$	Estimated delay samples
htx_{eff}	Effective antenna height of the transmitter
hrx_{eff}	Effective antenna height of the receiver
f	Carrier frequency
Lp	Propagation losses
ni,w	Number of indoor walls that the signal crosses
no,w	Number of outdoor walls that the signal crosses
nf	Number of floors that the signal crosses
L1,iw	Losses due to the indoor walls
L1,ow	Losses due to the outdoor walls
L1,fl	Losses due to the floor
Ψ	Fading losses
σ_f^2	Variance of the fading losses

1. INTRODUCTION

The mobile systems have been evolving since the first mobile generation was created in 1980s. These systems have had a great impact in the evolution of the society, technology, and in the last years, also in the business fields. In the first generation, only few people could afford to carry a mobile phone due to the high cost of the device and its unsuitable size. Nowadays, in the 4G era, the mobile phones are everywhere and are not used only for making voice calls, they are also used to access the Internet and the applications related with it. All these have led to an increase in the number of users and applications.

The growth of the applications brought the term Internet of Things (IoT). This term introduces the connection of different devices, which belong to different applications, to the network, i.e., not only humans will be connected to the network. Thus, a massive connection of devices has been foreseen, creating new network requirements to handle this fact and its consequences. These new requirements will be fulfilled with the new 5G mobile wireless system [2], [4]-[8].

The IoT is not the only reason for developing a new mobile system. The introduction of other technologies, such as cloud computing [62], [63] and big data [64], [65] have had a big impact in the decision. These new technologies have created some requirements that the current network architectures are not able to fulfil, e.g. a need for higher computing power and mobile connectivity at high speed. Users will be also influenced by the new technologies, they will not only consume data; users will become also data producers.

Among the new requirements, the localization or positioning of the devices is considered one of the key factors for the next mobile generation system [4], [6]. Until now, the positioning system has been an add-on feature to the standards, i.e., it has always been designed and optimized separately from the communication system. In the 5G mobile system, this will change: the communication and positioning systems will most likely be jointly designed and developed, giving support to the positioning natively [58], [59]. This is the topic that will be analyzed in this thesis.

When positioning and communication systems are jointly developed, it must be considered that each one of the systems has its own requirements. For the communication system, the optimization comes from the point of view of the data rate or capacity and the quality of service (QoS). However, in the positioning system, the timing accuracy is the key parameter of the optimization, which is directly related with the effective bandwidth

(i.e., the root mean square bandwidth or RMS BW) of the signal. In some cases, the RSM BW is low, and thus, the timing accuracy used for the positioning will be reduced.

An Orthogonal Frequency Division Multiplexing (OFDM) system splits the carrier frequency bands into many small frequencies, namely subcarriers, where the data is carried. To improve a low RMS BW, and considering an OFDM system, the subcarriers can be used to achieve the desired timing accuracy. However, if a big number of data subcarriers is allocated to the positioning system, less data subcarriers will be available for the communication, worsening the characteristics of the communication. Thus, both positioning and communications are impaired features, i.e., the performance of one feature improves at the expenses of the other one. Consequently, in 5G, two impaired features, positioning and communications, are wanted to be improved jointly.

In this thesis work, different metrics, which are explained in chapter 3 and 4, will be measured. With the obtained results, a performance analysis will be done for the joint communication and the positioning systems.

During this thesis, another issue has been considered, the one of finding out which 5G waveform is best suited for joint positioning and communication standards. Currently, there is no waveform defined for the 5G system due to the lack of the final standards. Different companies and entities are proposing different waveforms, such as: Wideband Cyclic-Prefix Circular Offset Quadrature Amplitude Modulation (WCP-COQAM), zero-tail - discrete Fourier transform -spread orthogonal frequency division multiple access (ZT-DFT-s-OFDMA), and cyclic-prefix orthogonal frequency division multiple access (CP-OFDMA).

In addition, with the introduction of the 5G system, new frequency bands have been proposed to be used, from 3 to 300GHz, namely millimeter wave (mmWave) band. As this kind of waves will provide a higher channel bandwidth, higher data rates will be achieved easily. In this project, this frequency band will be used to analyze the performance of the waves at these frequencies.

1.1 Objectives

The main objectives of this thesis have been to implement, using Matlab, a 5G transmitter-receiver system and the supporting channel models, which will be used to analyze the joint behavior of the communication and positioning systems. More detailed objectives were as follows:

- Understanding the need of developing a joint communication and positioning system, and identifying the needed performance metrics to analyze the system.
- Building some channel simulators valid for outdoor and indoor scenarios and able to serve some of the future 5G signals.

- Defining certain target criteria in terms of positioning and communication and optimizing the signal parameters in such a way that the best tradeoff among the target criteria is achieved.
- Investigating which of the currently proposed 5G waveforms (from various white papers and publications) are best suitable for both positioning and communication purposes.
- Computing the chosen performance metric of the communication and positioning systems jointly.
- Analyzing the obtained results by comparing the performance obtained with different waveforms and with the theoretical results obtained from the literature and getting the conclusions.

1.2 Author's contribution

In short, the main contributions of the thesis are the followings:

- The author collected and summarized the information about the current mobile system and their characteristics, as well as the different existing positioning systems.
- The author collected and analyzed the information about different 5G transmitters and receivers, and their implementation in Matlab, based on the following three waveforms: WCP-COQAM, CP-OFDMA, and DFT-s-OFDMA.
- The author implemented two channel models, one for outdoor scenarios and another one for the indoor scenarios. The outdoor channel model was based on the Mobile and Wireless Communications Enablers for the Twenty-Twenty Information Society (METIS) project [2]. The indoor channel model was based on a simplified path loss model included wall and floor losses in a 4-floor building of Tampere University of Technology.
- The author simulated the bit error rates (BER) and the Cramer Rao Lower Bound (CRLB) time error variance in order to study the positioning and communication performances, and also estimated the simulation-based positioning error. The positioning accuracy was analyzed at the link level, i.e., the distance estimation was implemented using one transmitter and one receiver and the estimated propagation time delay between the two only.

1.3 Structure of the document

This thesis is organized in 9 chapters as follows. In this first chapter, the introduction to the topic is done. It is explained also here the need for analyzing the joint communication and positioning systems simultaneously. In addition, the objectives of this thesis and the author's contributions are explained.

In chapter 2, the context of the field is explained, i.e., the evolution of the mobile communication systems since it began in the 1980s. Here, all mobile systems will be ana-

lyzed, including 5G and the future mobile systems (5G+). The analysis is done from two points of view, the communication and the positioning.

Chapter 3 explains the main targets that the 5G communication system needs to fulfil to reach the defined requirements in [4], [6], and [8]. Not all of these targets are analyzed in this thesis due to lack of time. The targets that are used in the thesis work are more extensively used

In chapter 4 the positioning and navigation requirements are explained for the 5G mobile system.

In chapter 5, the current literature about the joint communication and positioning systems is briefly explained. Also, the channel models that are used in the literature for 5G signals are overviewed.

In the two following chapters, 6 and 7, the simulation environment is explained, i.e., the whole simulator, the waveform generator, the channel models, and the performed changes. The basic graphical user interface (GUI) created in Matlab is also explained.

In chapter 8, the simulation parameters are explained and the obtained results are shown. This thesis ends by explaining the conclusions reached in this thesis work. The conclusions are shown in chapter 9, where some open issues and future work are also discussed.

2. EVOLUTION OF THE MOBILE SYSTEMS

In this section, the background of the mobile communication system is briefly explained, from the first generation of mobile systems, namely 1G or Advance Mobile Phone System (AMPS), until the present one, known as 4G or Long Term Evolution (LTE). The explanation is not limited to the communication systems, but the positioning is also explained, in case it is supported by the discussed communication system. After the background analysis, the main characteristics of the upcoming 5G systems are explained and the future of the mobile systems is discussed.

2.1 Evolution of the mobile communication systems

In the 1980s, the first mobile communication system was implemented, namely 1G. The main technologies used were: the AMPS in North America, the Nordic Mobile Terminal (NMT) in the Nordic countries of Europe and Russia, and the Total Access Communication System (TACS) in UK. Although all these technologies were mainly designed for voice calls, it was possible to send text messages by connecting the mobile terminal (MT) to an external device with a keyboard.

This first mobile system, 1G, was an analog system, a fact that affected to the QoS of the system. The presence of the noise during the transmission of the signal was a huge disadvantage. Thus, a new mobile wireless system was needed.

In the 1990s, a new communication system was implemented, namely 2G or the Global System for Mobile communications (GSM). In this new system, new features and technologies were introduced, but the main difference with 1G was that the system became digital. The modulation used in GSM is mainly Gaussian minimum shift keying (GMSK), even if in Enhanced Data rates for GSM Evolution (EDGE) enhancement of GSM, also the 8PSK modulation could be used [68]. This digitalization allowed to transmit more information in the same signal bandwidth, increasing the data rates to a maximum value of 384kbps [67].

2G is the first mobile system supporting user positioning to some extent. It was an add-on feature, i.e., it was developed separately from the communication system, and it was implemented after the 2G system. The accuracy obtained was of few hundred of meters [19], [21].

In the 2000s, together with the 2.5G and 2.75G systems, the 3G was introduced, also known as the Universal Mobile Telecommunication Service (UMTS). The 3G system

was implemented because a higher speed, higher capacity, and a good QoS were needed [17], [67].

The main features of 3G were the use of techniques based on spread spectrum, and the higher security. The spread spectrum techniques were used also in 2G, but 3G is mainly based on these techniques.

The introduction of the spread spectrum techniques in 3G allowed the use of a wider frequency band, increasing the bandwidth to 5MHz, which made possible to reach peak data rates of 48Mbps. As described in [3], this was achieved with the evolved High-Speed Packet Access (HSPA+), using the 64QAM modulation. HSPA is the evolution of UMTS, consisting in a collection of mobile protocols that improve the performance of the protocols of UMTS [67].

Regarding the positioning, in 3G there was not a specific waveform used solely for user positioning purposes. But the techniques used in 2G were improved, achieving a resolution of few tens of meters with the 3G system [19], [21].

Regardless of all the advantages obtained in the 3G systems, there were still some critical problems to be solved, such as the high-power consumption, low network coverage and high cost of the spectrum license. Adding these problems to an increased number of users, a new mobile wireless system was needed to provide a high quality, high capacity, and low cost services. For this purpose, an all-IP based system was build, namely the 4G mobile system.

The 4G system was implemented in 2011, replacing the spread spectrum techniques, acquired in the 3G system, by the Orthogonal Frequency-Division Modulation (OFDM) multi-carrier signals. This helped to achieve very high data rates despite the extensive multipath propagation. This kind of waveforms, which are based on efficient Fast Fourier Transform (FFT) algorithm and frequency domain equalization, made possible to control the bandwidth of the spectrum in a flexible way.

Regarding the positioning part, it is in the 4G when the system introduces, for the first time, specific waveforms for the user positioning, namely Positioning Reference Signals (PRS). PRS signals are used for Observed Time Difference of Arrival (OTDOA) User Plane Location Support (UPLS) and are transmitted with a periodicity of 160, 320, 640, or 1280ms [26]. At each transmission occasion, the position reference signals are sent in consecutive downlink subframes. More about OTDOA and PRS signals will be discussed later in this chapter.

The 4G system has functional limitations, such as not being able to provide services requiring both real-time response and big data sizes. Thus, the high-quality video experience that can be provided is limited to a number of users simultaneously. This is an inconvenience, considering that videos with a resolution of 4K (4000 pixels) and 8K

(8000 pixels) ultra-high definition (UHD) and holograms are expected to become popular and accessible in the future [2].

The introduction of the term IoT also had a big consequence in the 4G system context. This means that a huge number of devices will be connected to the network. In fact, the connected devices are expected to grow exponentially [25]. All these are translated in a need of a higher data capacity, so a new mobile wireless system will be needed soon.

The 5G mobile wireless system is expected to be implemented in the 2020s. Nowadays, there is no standard released, but there are many companies and entities working on the topic and many white papers have been published [4]-[7] . Despite the fact that there is no standard, the requirements to be fulfilled have been defined already. Some of the specific requirements for the 5G systems are shown below [6], [8]:

- Ultra-high reliability: it should be less than one packet lost out of 100 million.
- Ultra-low latency: it should be as low as 1ms.
- Ultra-high data rates: it should be multi-Gbps.
- Ultra-positioning: it should have an accuracy from 10m to less than 1m at 80% of occasions, and better than 1m for indoor deployments.

To achieve these requirements, new techniques will be needed, such as massive multiple input-multiple output (MIMO), mmWaves, and machine-to-machine (M2M) connectivity. M2M will allow the communication between machines or devices without the need for the human interaction, this kind of applications is directly related to the IoT.

Massive MIMO and mmWaves technologies[1] have a number of favorable properties, and this is the reason for adopting them in the 5G system. For example, the use of carrier frequencies operating above 30GHz will allow to use larger bandwidths [9]. But still there are several challenges related to the mmWaves. The main problem is that, because of the higher carrier frequency, the propagation loss is relatively higher compared to other communication systems [11].

Having a relatively high frequency, means that the wavelength is relatively small, they are inversely proportional, $\lambda = \frac{c}{f}$. A small wavelength means that the system is more vulnerable to various interferences and it is easier to suffer blockage or shadowing, degrading severely the performance of the system [11]. Other effects such as rain attenuation and atmospheric and molecular absorption are also relatively higher in the case of mmWaves [11].

The waveforms to be used in this system are not specified yet. There are some proposals as the ones that are used in this this thesis: wideband cyclic-prefix circular offset quad-

[1] mmWaves: millimeter-waves are electromagnetic waves that are located in the frequency spectrum between the 30 and 300GHz. In this frequency band, the available bandwidth is higher, up to 7GHz in some countries [11].

rature amplitude modulation (WCP-COQAM) [12], [15], zero-tail discrete Fourier transform-spread orthogonal frequency division multiple access (ZT-DFT-s-OFDMA) [13], [14], [71] cyclic-prefix orthogonal frequency division multiple access (CP-OFDMA) [15], [16], [71], filtered OFDM (F-OFDM) [69], windowing OFDM (W-OFDM) [69], filter bank multicarrier (FBMC) [12], [15], [16], [69], universal filtered multicarrier (UFMC) [12], [72], filtered multitone (FMT) [70], Universal filtered OFDM (UF-OFDM) [12], [71], and generalized frequency domain multiplexing (GFDM) [73].

In the future 5G system, the positioning will most likely not be an add-on feature, i.e., the communication and positioning systems will be implemented and developed at the same time. This is because the positioning has become one of the main features in some future applications. The main applications of the positioning in 5G are the autonomous cars, and for that, many different waveforms have been proposed in [16] for these specific applications.

The next mobile wireless system to be implemented will be the 6G system. In this generation, the 5G mobile system will be integrated with the satellite network [17], [18]. The satellite network will be comprised by three satellite networks: telecommunication satellite network, Earth imaging satellite network, and navigation satellite network. The telecommunication satellite network allows the data, internet, video and voice broadcasting. The second one, the Earth imaging satellite network, is the one that collects information about the weather and the environment. Finally, the last satellite network, is the one used for the global positioning, that is comprised by four systems: GPS (USA), Galileo (Europe), GLONASS (Russia), and COMPASS (China).

Integrating all these four networks means that the satellite systems and the mobile system will have to be interconnected. Therefore, the main problem to be solved in this generation will be the handover and the roaming [17], [18].

Even if the 6G system will support local voice coverage and other services, in the 7G system, there will likely be a research on issues such as the use of mobile phone during moving conditions from one country to another [17]. In this situation, it has to be considered that the satellites are also moving in a constant speed and in a specific orbit. The research will also be oriented to the standards and protocols related to the satellite to satellite and mobile to satellite communications. So, in 7G the mobile and satellite network will offer a global coverage and will define the satellite functions for mobile communications [18].

Once 7G is implemented, the data capacity, coverage, and handover problems will be most likely solved. However, a new issue will be present: the cost of the mobile phones, the calls, and the services. This is an issue that further (7G+) mobile communication systems will have to manage [17], [18].

In Table 1, the comparison between the different generations of mobile systems is shown. Future mobile generations are taken into consideration.

Cellular generation	**1G**	**2G-2.75G**	**3G-3.75G**	**4G-4.5G**	**5G**	**5G+**
Added features respect to the previous generation	-	Digital modulation	Higher security, spread spectrum	OFDM modulation, MIMO, smart antenna arrays	mmWave, massive MIMO, M2M connectivity	Interconnection between mobile and satellite networks
Technology	AMPS, TACS, NMT	GSM, IS-95, GPRS, EDGE	UMTS, HSPA, HSPA+, CDMA2000	LTE	To be defined	To be defined
Carrier Frequency (GHz)	0.15 and 0.8	0.8, 0.9, and 1.8	0.85, 1.9, and 2.1	0.7, 0.8, 0.9, 1.8, and 2.6	1-100	To be defined
Bandwidth (MHz)	0.03	0.2	5	1.4-20	To be defined (hundreds)	To be defined
Modulation	FM	GSMK, 8PSK (EDGE)	BPSK, QPSK, 16QAM, 64QAM	4QAM,16QAM, 64QAM	To be defined	To be defined
Multiple Access	FDMA	TDMA, CDMA	WCDMA	OFDM, SC-OFDMA	To be defined	To be defined
TDD/FDD	FDD	FDD	Both	Both	Both	To be defined
Data rates	2-14.4kbps	64-384kbps	2-48Mbps	1Gbps	10Gbps	To be defined
Latency (ms)	-	>150	100	50	1	To be defined
Positioning supported?	No	Yes, add-on feature	Yes, add-on feature	Yes, add-on feature	Yes, native support	Yes, native support
Positioning waveforms	No	No	No	Yes (PRS)	Yes (to be defined)	Yes (to be defined)
Positioning accuracy	-	Few hundred meters	Few tens of meters	Few meters	<1m	To be defined
Services	Voice calls	Digital voice, SMS, narrowband Internet	Video conferencing, mobile TV, broadband Internet	Real-time applications, ultra-broadband Internet	4K-8K UHD video, telesurgery, autonomous cars	To be defined

Table 1: Comparison between the different generations of mobile system

2.2 Positioning methods in cellular networks

The 2G mobile wireless system was the first cellular system introducing the user positioning as an add-on feature. Since then, many methods have been developed in order to

implement the user positioning, but the most important ones are shown in Table 2, with the approximate accuracy that can be reached in each method [19]-[21]:

Technology	Urban env.	Rural env.
CGI	>100m	<35km
RSS	>100m	30m
CGI+TA	>100m	550m
UL-TOA	150m	50m
U-TDOA	50m	80m
IP-DL OTDOA	>100m	20m
E-OTD	200m	60m
A-GPS	20-30m	3-10m
5G (to come)	<1m	1 m

Table 2: Main cellular positioning technologies and their accuracy

All these positioning systems are divided in two categories, network-based positioning systems and mobile station-based positioning systems. Among the network-based positioning systems, the following positioning methods can be found: Cell Global Identity (CGI), Received Signal Strength (RSS), Angle of Arrival (AOA), Timing Advance (TA), CGI+TA, Uplink Time of Arrival (UL-TOA), and Uplink Time Difference of Arrival (U-TDOA). The mobile station-based positioning systems are represented only by the Observed Time Difference of Arrival-Idle Period on the Downlink (OTDOA-IPDL), Enhanced observed time difference (E-OTD), and Assisted GPS (A-GPS).

2.2.1 Network-centric positioning system

CGI is the most basic and imprecise method for positioning, but it can be very useful in case other methods fail [20], [21]. This method consists in obtaining the identification of the cell in order to locate geographically the mobile terminal (MT).

Another method is implemented by the use of the received signal strength (RSS). When a signal is received, its strength can be used to estimate the location of a MT. Considering that theoretically the signal strength can be calculated as shown in (1) [22]:

$$RSS = T_x - (L_{LS} + L_{MS} + L_{SS})\ [dB], \qquad \textbf{(1)}$$

where T_x is transmitted signal strength, L_{LS} is the attenuation due to large-scale propagation effects (i.e., path loss), L_{MS} is the attenuation due to medium-scale propagation effects (e.g. shadowing), and L_{SS} is the attenuation caused by small-scale propagation effects (e.g. multipath).

In RSS based positioning methods, it is considered that the strength of the signal decreases exponentially as the distance increases. However, there are many objects that can disturb the signal, and thus, the accuracy obtained with positioning methods based on RSS is very low.

Regarding the L_{LS} in (1), for outdoor environments, the path loss can be calculated for example using Hata's model, which is developed for macrocells on the experimental results of Okumura [23]. It can also be calculated using the free space loss formula shown in (2).

$$FSL = 20\log_{10}\left(\frac{4\pi d}{\lambda}\right), \qquad \textbf{(2)}$$

where λ is the wavelength of the carrier frequency and d is the distance between transmitter and receiver.

The losses caused by medium-scale propagation, i.e., shadowing, are calculated using Gaussian statistics [22]. Finally, the losses caused by small-scale propagation, i.e., multipath, can be modelled using the Rayleigh distribution [22].

Another common positioning method is the Angle of Arrival (AOA). This helps to improve the positioning obtained by locating the receiver within a section of the entire cell. This section will be delimited by the estimation of the received signal's direction, and thus, directional antennas are needed for a high accuracy. To estimate the user position, at least two base stations or access nodes are needed with directional antenna or antenna arrays [20], [21], [24]. In AOA, the intersection of 2 lines of direction defines the position where the MT is supposed to be located. The method is illustrated in the figure below:

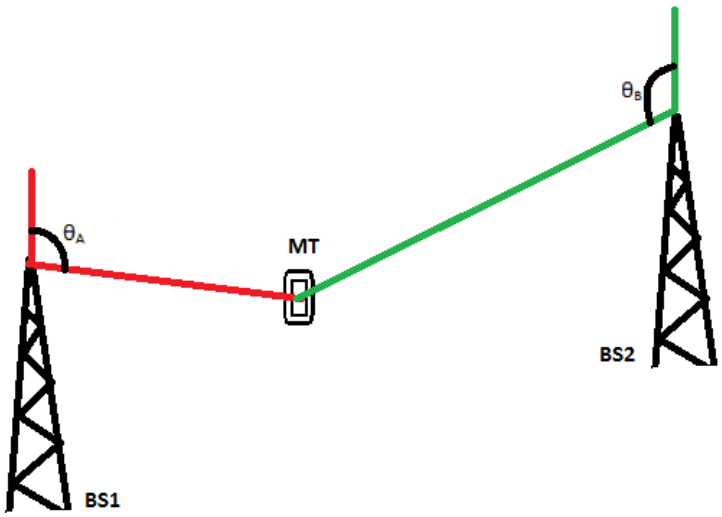

Figure 1: AOA method

The Timing Advance (TA) is another positioning method based on the propagation delay compensation [20]. This technology is based on the Time Division Multiple Access (TDMA) characteristic, where different time slots are assigned to different users. To arrive at the correct time, the MT must send the data earlier, and this amount of time is calculated by the base station (BS) and communicated to the MT. The TA is directly

related to the distance between the MT and the BS. If TA is combined with CGI (CGI+TA), the position of the MT will be confined to an arc of a circle with a resolution of 550m.

The Uplink-Time of Arrival (UL-TOA) is a better or more accurate positioning method. To be implemented, at least four BSs need to be close to the MT [20], [21]. The time of arrival measurement method is shown in Figure 2.

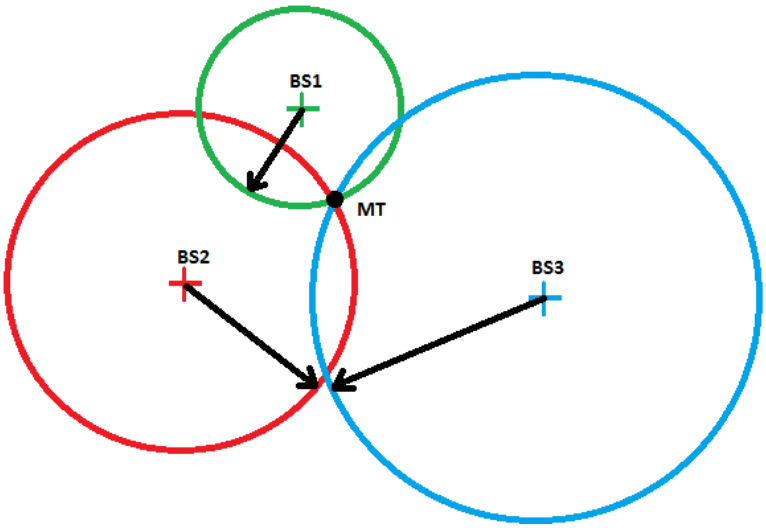

Figure 2: Time of Arrival method

In the Time of Arrival (TOA) technique, the measured signal propagation delay is used in order to calculate the distance between BS and MT.

TOA assumes the LOS propagation, drawing a circumference at the calculated distance, as shown in Figure 2. If two BSs are used to estimate the position in two dimensions, two circumferences would be calculated, and the intersection of two circumferences would give generally two points, so there is ambiguity in the user position. Thus, at least 3 BSs are needed to estimate the user position in 2D, and at least 4 for 3D positioning. To implement this method, the positions of the BSs must be known also [20], [21]. For positioning the expression in (3) is used per each received signal.

$$d_i = c \cdot (T_i - T_0) + \varepsilon_b = \sqrt{(x - x_i)^2 + (y - y_i)^2 + (z - z_i)^2} + \varepsilon_b, \qquad \textbf{(3)}$$

where d_i is the distance between the transmitter and the i –th receiver, and c is the speed of light. The transmission and reception time are given by T_0 and T_i, respectively, and they are needed to estimate the propagation delay. The position of the i –th BS is given by (x_i, y_i, z_i), and the unknown position of the MT by (x, y, z). It is possible to calculate the position of the MT in two dimensions by removing from (3) the term $(z - z_i)^2$. When using the expression above, there is a distance error introduced by the clock bias, i.e., there is a time difference between the transmitter and the receivers. This distance error represented with the term ε_b.

During this thesis, the distance estimation between a BS and the mobile station will be calculated based on TOA measurements. The estimated propagation delay will be calculated with the autocorrelation and the delay obtained in samples will be translated into the distance estimation. More about this will be explained in the chapter 6.

Another network-based positioning method is the Uplink-Time Difference of Arrival (U-TDOA). The principle is the same as with UL-TOA, but instead of using the propagation delay, it uses the propagation delay differences. These propagation delay differences are translated in distance differences, and the distance differences will define several hyperbolas. The intersection of different hyperbolas will give the position of the MT.

The distance difference between two BSs is given by the expression below:

$$\Delta d_{i,j} = d_i - d_j = c \cdot (T_i - T_0) - c \cdot \left(T_j - T_0\right) = c \cdot \left(T_i - T_j\right) = c \cdot \Delta T_{i,j}, \qquad \textbf{(4)}$$

where $\Delta T_{i,j}$ is the propagation delay difference. The advantage of this method is that there is no need to use the time of the BS (T_0) [19].

2.2.2 Device-centric positioning systems

Regarding to the device-centric positioning, there are three main methods: Idle Period Downlink- Observed Time Difference of Arrival (IPDL-OTDOA), Enhanced Observed Time Difference (E-OTD), and Assisted-Global Positioning System (A-GPS). The first one is very similar to U-TDOA, but it works in the other way round, i.e., it is a downlink technique, where the positioning is computed at the MT side, based on the observed time differences. In this case, the synchronization bursts are used for estimating the position of the MT [22].

The Assisted Global Positioning System (A-GPS) is the most accurate method used for user positioning in cellular systems, according to [21], [22]. This method uses at least 4 satellites. A-GPS uses the mobile network to send corrections to the MT regarding ephemeris, ionospheric delays, tropospheric delays, etc. [20]-[22]. The network tells the MT which satellites are in view, by providing their approximate positions and clock times. With this information, the MT can start to calculate the position immediately (the acquisition search space becomes lower than for non-assisted case). This way, the performance and power consumption are greatly improved [22].

In the 4G system, the Observed Time Difference of Arrival (OTDOA) method was implemented with the help of the PRS signals to calculate the user positioning, another device-centric positioning method. In OTDOA, the Reference Signal Time Difference (RSTD) measurement is calculated. The RSTD defines the relative timing difference

between two cells, the reference cell and a measured one [26], and the expression is given in (5).

$$RSTD_{i,1} = \frac{\sqrt{(x_t - x_i)^2 + (y_t - y_i)^2}}{c} - \frac{\sqrt{(x_t - x_1)^2 + (y_t - y_1)^2}}{c} + (T_i - T_1) + (n_i - n_1), \quad \textbf{(5)}$$

where $(T_i - T_1)$ is the transmit time offset between the two BSs, and n_i and $n_1$are the TOA measurement errors between the MT and the two BSs.

To implement OTDOA for 2D positioning, at least two neighbor cells measurement are needed, which gives two equations with two unknowns (x_t, y_t). For this method, it is assumed that the coordinates of the BSs (x_i, y_i) and the transmit time offsets $(T_j - T_i)$ are already known. In a synchronized network, the term $(T_i - T_1)$ of the equation above should be zero, defining this way the TDOA positioning method. The distance accuracy achieved is of the order of ten meters, according to [26] where they showed an achievable OTDOA error of 9.8m.

OTDOA can be implemented with any downlink signal, e.g., synchronization signals, but it suffers from poor hearability [26]. To solve the problem, PRS signals have been introduced in 4G, allowing proper timing measurements, and thus, improving the positioning performance of OTDOA. PRS signals are pseudo-random QPSK sequences [26]. OTDOA is also used in 3G networks. In there, the hearability problem is solved via an Idle Period Down-Link (IP-DL) transmission [21].

3. COMMUNICATION TARGETS

In this chapter, the typical communication targets for a good performance of the 5G communication system will be overviewed. Once the targets are defined, the mathematical definition or measurement method will be discussed regarding how such target performance criteria are computed. During this chapter, five applications that will likely be implemented in the 5G system will be explained and connected to the communication targets.

3.1 Key performance indicators for communication targets

The communication targets are quite difficult to define in a comprehensive manner, because for each type of applications, different targets are considered. Thus, accomplishing this task is not easy, because future applications need to be also considered when targets are defined. To increase even more the difficulty of this task, the Internet of Things (IoT) communications will be supported in the 5G system, which means that a massive connection of devices is expected [25]. These devices will need to fulfil different targets, which will depend on their working purpose, i.e., in what they are being used. All these new types of applications must also be taken into consideration when defining the communication targets.

To simplify the definition of those targets, each company and/or entity have made a classification of the different services. Some examples of this classification are shown below:

- **5G HyperService Cube:** is the classification made by Huawei in [5]. In this classification, the services are located inside a cube where each axis represents the throughput, the number of links, and the delay of the service needed for each application or service, respectively.
- **Service and technical challenges**: are the two classifications made by 5G Forum in [4]. The different applications and services are grouped inside general services, which are: Mobile Contents Streaming Services, Social Knowledge Sharing Services, High-Density User Services, Smart Transportation & Robots Services, Public Safety Services and 5G Extension Services for Avionic, Maritime and Space Communications. After this classification, the general services are linked to at least one of the following technical challenges: hyper-transmission, hyper-connectivity, hyper-mobility, hyper-response, hyper-positioning, hyper-reliability, hyper-energy saving, and hyper-cost effectiveness.
- **Scenarios with extreme use cases:** is the classification made by METIS [27]. In this classification, METIS defines the challenges to be solved in applications

with extreme needs, and this way, it defines also the goals of the 5G system. The scenarios are the following ones: amazingly fast, great service in a crowd, ubiquitous things communicating, best experience follows you, and super real-time and reliable connections.

When a service or application is going to be evaluated, the success of the service or application is analyzed, i.e., the performance is measured. To realize these measurements, some key performance indicators (KPIs) are defined.

In this thesis, the performance of the 5G system is going to be analyzed for 3 different waveforms, and from the point of view of the communication and the positioning system. So, regarding to the communication targets, the KPIs that are defined for the 5G system [27] are shown in Table 3.

KPIs	**Measurement parameters**
Traffic volume density	Data volume per area unit
Experienced end-user throughput	Data throughput
	Data rate
Latency	One-way Trip Time(OTT) latency
	Round Trip Time (RTT) latency
Reliability	BER
	SER
	PER
	SNR
	SINR
	Outage probability
Availability and retainability	Availability
	Retainability
Energy efficiency	Spectrum efficiency
	Energy efficiency
	Energy per information bit
	Power per area unit

Table 3: KPIs defined for the 5G system

The first KPI is the traffic volume density. This KPI describes the total data volume transferred to/from the user equipment during a predefined time period in a given area. The area will be defined by the area covered by the radio nodes, that will belong to the Radio Access Network (RAN) [27].

It has been stated in [27] that the 5G system will have to support 1000 times higher traffic volume density compared to today's network. This increase has been defined considering the expected growth of mobile traffic volume [27].

There is not a mathematical way of defining the traffic volume density, but it can be computed in an empirical way. The computation is done by summing the traffic volumes that has been produced by a user equipment, and then dividing it by the overall service area. This traffic volume will strongly depend on the environment and user density, and on the day time.

The second KPI, namely the experienced end-user throughput, is the data throughput a user achieves in the MAC layer averaged during a predefined time period. The data considered for the throughput calculation is the one belonging to the user plane only. This KPI can be used to measure the quality of experience (QoE) level of the user for a certain service. The experienced throughput depends on the number of users and the amount of data they generate. The main goal is to increase the data rate from 10 to 100 times [27].

For a mathematical definition, let's consider that the user i have the packet k, which is $L_{i,k}$ bits long. If the end-to-end delay is $T_{i,k}$, the throughput for this packet is defined as follows: $R_{i,k} = L_{i,k}/T_{i,k}$. Thus, the expected packet throughput is calculated with the expression shown in (6).

$$Th_i = E_k\left[R_{i,k}\right] = E\left[\frac{L_{i,k}}{T_{i,k}}\right], \tag{6}$$

where the expectation is taken over a time period specific to the application.

In MIMO, and thus, beamforming environments, the achievable data rate can be measured as a metric for the end-user throughput. For that the expression in (7) is used.

$$R = E\left[W_{data}\log_2\left(1 + \mathbb{1}_{align}\cdot SNR_{data}\right)\right], \tag{7}$$

where, W_{data} is the total available bandwidth, $\mathbb{1}_{align}$ is the indicator function of beam alignment, and SNR_{data} is the Signal-to-Noise ratio (more about this expression in [75]).

Regarding to the latency, two different types are defined, the end-to-end (E2E) latency, or one-trip time (OTT) latency, and the round-trip time (RTT) latency. The OTT latency refers to the time a data packet needs to cross the network. This measurement considers the transmission time of the packet and the reception time. This measurement is achieved in the link layer, the delays added by the MAC layers are not considered [27].

The RTT latency, unlike the OTT latency, measures the time that a packet need to reach to its destiny and the time that is needed to receive the acknowledgment of the transmitted packet. This measurement, alike the OTT latency, is also achieved in the MAC layer, without considering the higher layers [27].

The goal to reach with the 5G technology is to provide a 5 times reduced OTT latency compared to the latency obtained in 4G. When the latency is measured, it must be considered that the entire network has effect in the latency.

To define the latency mathematically, as it is done in [27], two peers, which can be a BS and a MT, two BSs, or even two MTs, are considered, peer 1 and peer 2. The transmission of the data packet will start in the instant T_{S1} from the peer 1, and will be received

at the instant T_{A2} in the peer 2. With this information, the OTT latency can be calculated by using the expression (8).

$$T_{OTT} = T_{A2} - T_{S1}. \quad \textbf{(8)}$$

After the data packet is received in the peer 2, the acknowledgement packet will be sent back to the peer 1. Considering that the acknowledgement packet is received in the peer 1 at the instant T_{A1}, the RTT latency can be calculated with the expression in (9).

$$T_{RTT} = T_{A1} - T_{S1}. \quad \textbf{(9)}$$

The reliability is used to describe the quality of a radio link connection from the service point of view, i.e., describes the QoS of the radio link. There are many different metrics that help to analyze the QoS of a service at the PHY/MAC layer, such as signal to interference plus noise ratio (SINR), bit error rate (BER), symbol error rate (SER), packet error rate (PER), and outage probability.

The SINR gives the ratio between the power of the received signal and the sum of the interfering signal and the background noise powers. This metric will measure how much signal you have relative to your noise and interfering signals. This metric is usually expressed in dB. The SINR is calculated with the expression below [28]:

$$SINR = \frac{P_{RX}}{P_{AWGN} + \sum_i P_i}, \quad \textbf{(10)}$$

where $P_{RX}$is the power of the received signal, P_{AWGN} is the power of the additive white Gaussian noise, and P_i is the power of the i-th interfering signal. In this thesis, the interferences have not been considered; only the additive white Gaussian noise has been considered; more about this is given in chapter 6.

The bit error rate (BER), which is another possible performance criterion, compares the bits obtained from the received signal with those that are transmitted. Some of the bits obtained in the receiver may be different from the transmitted bits, which are considered errors. These errors can be caused by different effects, such as the channel noise, interferences, distortion, attenuation, wireless multipath fading, and bit synchronization problems. In this project, different SNR values have been selected to analyze the evolution of the BER in function of the SNR. More about this is shown in chapter 6.

Considering that interferences and channel noise affect the SNR and SINR, there is a relation between these three metrics. The noise power affects both SINR and SNR, by decreasing them, and thus, by increasing the probability of having mismatches between the transmitted and received bits.

The Symbol Error Rate (SER) and the Packet Error Rate (PER) are similar to the BER. The difference in the SER is that the ratio gives the number of symbols that are received

with error. The PER, however, gives the ratio of packets that have been receiver with error. The BER, SER, and PER are carried out within a predetermined time period.

The outage probability defines the amount of time in which the service condition is below to a defined system operational threshold, i.e., the given service performance is below an acceptable performance level [27].

The service availability describes the percentage of places within a coverage area where the service is provided to the end user with the requested Quality of Experience (QoE) level. It can also be described as the percentage of communication links that can fulfil the QoE requirements within a geographical area.

The retainability, which is a special aspect of the availability, analyses if a service has been made available whenever the user needs it.

Within the IoT systems, there is going to be a massive deployment of sensors, that will work with batteries, so energy efficiency is a KPI that must be considered. Reducing the energy consumption of the BSs is also an important consideration of the energy efficiency [29].

The energy efficiency is defined as the aggregate bit rate that is achievable over 1Hz nominal bandwidth while consuming a given power. The mathematical expression for the energy efficiency is given in [30]:

$$E_{eff} = \frac{NSE}{network\ power\ consumption\ over\ 1km^2} \quad \textbf{(11)}$$

where NSE is the network spectrum efficiency.

The network spectrum efficiency is the network-level spectrum efficiency measure, which depends on the spatial reuse within an area. The mathematical expression for this is also given in [30]:

$$NSE\left[\frac{kb}{s}/\frac{Hz}{km^2}\right] = (cell\ spectrum\ efficiency) \cdot (cell\ density\ over\ 1km^2) \quad \textbf{(12)}$$

where the cell spectrum efficiency can be calculated by the use of the Shannon capacity bound.

Another way of measuring the energy efficiency is by using the energy per information bit and the power per area unit [28]. The energy per information bit is widely accepted for urban environment, and the mathematical expression is shown below:

$$\lambda_I = E/I = P/R \text{ in [J/bit] or [W/bps],} \quad \textbf{(13)}$$

where E is the consumed energy in a given observation time period T, P is the consumed power, I is the information volume, and R, the information rate. All the parameters used in the expression above are measured at the MAC layer.

The power per area unit, is typically applicable in suburban or rural environments, and the expression is shown below:

$$\lambda_A = P/A \text{ in } [\text{W/m}^2], \qquad \textbf{(14)}$$

where P is the power consumed, and A is the covered area.

3.2 Application examples

With the introduction of the 5G system, new applications will be introduced. In this section, five of them will be briefly explained and they will be linked to few of the communication targets mentioned above. The communication targets that will be used in this thesis are: BER, data rate, latency, and the energy efficiency. The positioning targets will be described in Chapter 4.

Regarding to the 5G applications, five applications are selected for the discussion here: i) autonomous cars, ii) flying drones, iii) remote surgery, iv) wearable sensors, and v) public safety services. In Figure 3, the relation between the applications and the targets is shown according to the Author's view. A low level means that a certain performance criterion is not very important for that particular application, while a high level means that such a performance criterion is very important in the context of the target application. As it can be seen in Figure 3, different applications have different requirements. For example, low latency is crucial is public safety applications, while positioning accuracy is highly needed for autonomous cars, or remote surgery.

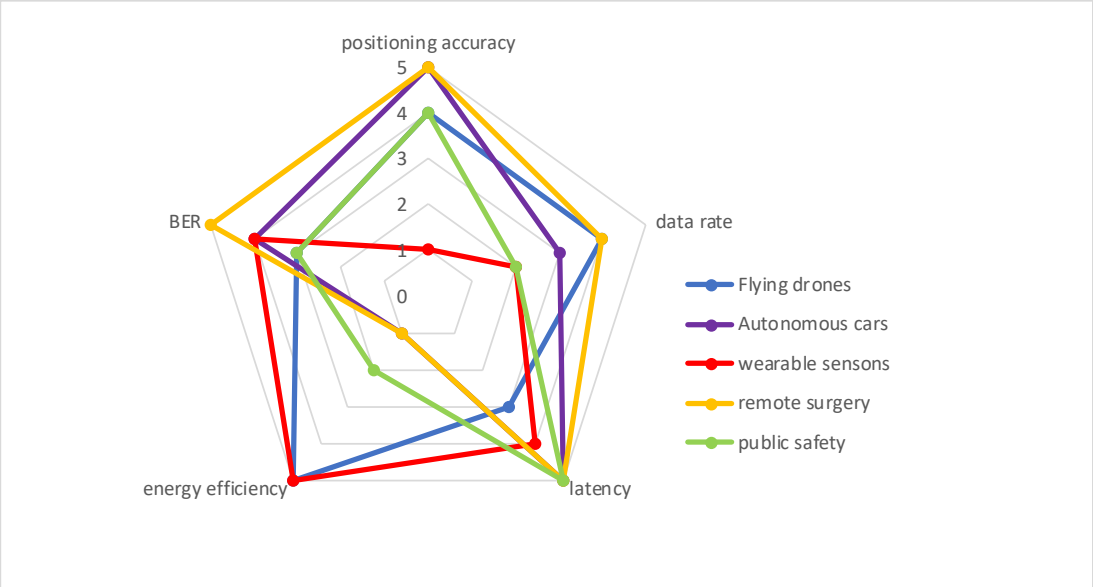

Figure 3: 5G application examples and their communication targets

The flying drones are used in many applications, such as packet delivery and video recording in festivals and concerts. The positioning of the drone need to be accurate in case a packet need to be delivered, and also it is important when a video is being recorded, thus we estimated a positioning need on level 4 (out of 5) for the drones applications. The communication exchange between the drone and the controller is huge, explicitly when a video is being recorded. Thus, the data rate should be high. The most important metric in a drone is the energy efficiency, the more energy efficient, the longer will be the battery duration.

The autonomous cars are another of the current and most interesting applications for the 5G system. These are cars that do not need the interaction with the driver to reach a predefined location. Autonomous cars are equipped with a variety of sensors that will be used to avoid collisions between cars or between cars and the environment, so they will need to read the surrounding environment at every moment. The position of the car is a key factor for the collision avoidance system, which will use the position of the autonomous vehicle and the information provided by the surrounding vehicles. The information provided will contain the position of the vehicles. In this kind of application, the data exchange is not high, so there is no need for a high data rate, but the low latency is a key factor.

The wearable devices are small chips that will be used for example while doing sport to monitor the heart rate. This kind of devices do not send too much information, so the required data rate is low, but latency and the energy efficiency are key factor for this kind of devices. Continuing with the heart rate example, the better the latency, the faster will be updated the information about the heart rate that is being monitored. In addition, the better the energy efficiency, the longer will last the battery of the device.

The remote surgery is a critical operation. With this application, the doctor will not need to be present in the surgery room to perform the surgery. It could be done remotely, with a robot in the surgery room that repeats the exact and precise movement that the doctor does. For this application, the positioning, data rate and latency are key factors, but also the BER is important if a lot of signaling or controlling data is to be exchanged. The minimum or a small error could trigger a fatal medical negligence.

Finally, it is necessary to have a good positioning information of the emergency calls, so the positioning and the latency are critical factors in the good performance of these services. Positioning targets are discussed in the chapter 4.

4. NAVIGATION AND POSITIONING TARGETS

In chapter 3, different KPIs were introduced for the communication targets. In this chapter, the KPIs for the navigation and positioning targets will be explained. Similar to the communication system, there are some error sources that affect the performance of the positioning. In this chapter, also the error sources in positioning will be briefly explained.

To analyze the QoS for the positioning, there are several performance indicators that must be considered. The main KPIs are the positioning accuracy and response time [32]-[34]. There are also other KPIs that should also be analyzed, such as reliability, availability, and the energy efficiency in the context of the positioning engine [34].

4.1 Accuracy

The positioning accuracy defines how close the estimated user or terminal location is to the real location of the MT. The closer the measured location to the real one, the more accurate is the measurement [34]. To evaluate the accuracy, the square root-mean-square error (RMSE) is measured, which can be calculated with the expression below [34], [35], [42]:

$$RMSE = \sqrt{\frac{1}{N}\sum_{k=1}^{N}([\hat{x}_k - x]^2 + [\hat{y}_k - y]^2 + [\hat{z}_k - z]^2)} \qquad \textbf{(15)}$$

where N is the number of measurements and k is the measurement index. The RMSE measurement depend on the real position of the device, (x, y, z) and in the estimated, or measured, position, $(\hat{x}_k, \hat{y}_k, \hat{z}_k)$.

The accuracy, can be measured in horizontally or vertically, namely two-dimensional (2D) and three-dimensional (3D) accuracy, respectively [31], [34], [36]. The horizontal accuracy is mainly used in mobile positioning, where the altitude is sometimes ignored [51], [76] . The vertical accuracy refers to the height of the MT.

The error probability of the distance error can also be used to set limits for the maximum accuracy error that is allowed. In the 2D cases, the circular error probability (CERP) is used [34], and for the 3D cases, the spherical error probability (SERP) is used [34]. For the 5G system, it has been stated that for the 80% of the time, the outdoor accuracy must be from 10m to less than 1m, and that for indoor scenarios, the accuracy must be below 1m [6].

In this project, the range estimation is achieved based on the signal propagation delay between a transmitter and a receiver. This estimation accuracy can be modeled also by using a Cramér-Rao lower bound (CRLB), which gives the achievable variance of any unbiased estimator [37]. For distance estimation in this thesis, the CRLB will be defined with the expression below [37]:

$$\sigma_{CRLB}^2 = \frac{c^2}{8\pi^2\beta^2\frac{E_s}{N_0}} \tag{16}$$

where c is the speed of light, β is the equivalent signal bandwidth and $\frac{E_s}{N_0}$ is the SNR. The equivalent signal bandwidth is calculated using the following expression [37]:

$$\beta^2 = \frac{\int f^2|S(f)|^2 df}{\int |S(f)|^2 df} \tag{17}$$

where $|S(f)|^2$ is the power spectral density function (PDF) of the transmitted signal. As proposed in [39], the two-dimensional or horizontal accuracy can be estimated using the CRLB for the estimated distance in the x axis and in the y axis. This method is proposed for DOA measurements and is given in the expression (18).

$$RMSE \geq \sqrt{CRLB_x + CRLB_y} = \frac{d \cdot \sigma_\varphi}{\sqrt{2}} \tag{18}$$

where d is the inter-site distance between two access nodes and σ_φ is the standard deviation of the DOA estimation error.

In many occasions, the lower bound that is estimated with the CRLB cannot be directly calculated with the given expressions (16) because there are many unknown parameters, e.g. in multipath environments, or when many transmitters are used. To overcome with this problem, the Fisher information matrix (FIM) can be used, as for example in [38], [40], and [41]. In addition, in [40] the CRLB expressions can be found for DOA, RSS and hybrid DOA-RSS positioning estimation.

4.2 Response time or latency

The response time, also named latency, is another of the parameters that measure the QoS of the navigation or positioning system. The latency, in the positioning context, defines the time since the position is requested, until the response is received with the estimated position [33]. The requirement of small latency will depend on the application type. There are many applications that need the location at the same instant it has been requested (real-time positioning). Such applications are also referred to as the “no delay” applications [36]. In the “no delay” applications, either initial or last known loca-

tion of the MT is provided. If there is no available positioning estimation, an error message will be delivered and the procedures to obtain a position estimation will start, i.e., the positioning engine will restart.

If the application can support a low-level delay, when the position is requested, the estimation will be calculated and sent back as soon as possible. In such applications, where a certain positioning delay can be tolerated, the positioning accuracy requirements may not be fulfilled due to the fast calculations [36].

Finally, there are some applications that can tolerate high delay. For these applications, the MT will receive the requested information always with the accuracy requirements fulfilled [36].

The latency can also be defined as the time needed since the power-up of the MT is achieved, until the first location measurement is obtained [34].

4.3 Availability and reliability

The availability defines the percentage of the total coverage area in which the required accuracy is achieved [77]. The factors that affect to availability of the positioning system are many and have different effects, such as: the cell coverage, the geometry of the BS, and the signal propagation environment [34]. The availability can be measured with the expression shown in (19), which is provided by the authors in [77].

$$Availability = \frac{num}{total}\ x\ 100\%, \qquad \textbf{(19)}$$

where num is the number of measurement points where the obtained positioning accuracy fulfils the required accuracy, and $total$ is the number of total positioning points.

The reliability reflects the ability of resisting huge measurement errors, and thus, the reliability gives the ratio of successful positioning attempts out of all attempts that have been made [34]. The positioning should be extremely reliable, and even more in emergency cases. If the positioning systems fail quite often, or the estimated position is false, user will not trust in the positioning system. As it is proved in [32], the reliability is dependent on the time of the day.

4.4 Power consumption of the positioning algorithm

The power consumption is another of the parameters to consider when analyzing the performance of the positioning or navigation. This is measured in the MT, and thus, it depends on the positioning method that is being used [31]. If the used positioning method is network-based, i.e., the calculations are carried out in the network and not in the MT, the power consumption will be low. Otherwise, if the position estimation is

carried out in the mobile terminal, it will be using its own resources, increasing the power consumption.

Once analyzed the different KPIs, a how they are related with the positioning, it is possible to related the positioning methods explained in chapter 2, with the KPIs explained in this chapter. An example of these relations can be seen in the table below, based on Author's understanding:

	Coverage, Availability	**MT power consumption**	**Latency**
AOA	Ubiquitous	Low	≈10s
RSS	Ubiquitous	Low	<5s
CGI	Ubiquitous	Low	≈10s
CGI+TA	Ubiquitous	Low	<5s
UL-TOA	(Sub)urban	Medium	<10s
U-TDOA	(Sub)urban	Medium	<10s
IP-DL TDOA	(Sub)urban	Medium	<10s
E-OTD	(Sub)urban	Medium	<10s
GPS	Ubiquitous	Very high	<35s
A-GPS	Outdoors	High	<5 s
5G (to come)	Ubiquitous	Very Low	< 1s

Table 4: Positioning methods with corresponding availability and consumption

4.5 Error sources in positioning

Considering all the error sources, it is possible to classify them into three main groups, as shown in [44]: errors due to the wireless environment, errors due to the geometry of topology of the environment, and errors due to the computations and/or measurements processes. Among the error sources of the first group, wireless environment, is possible to identify different factors that affect physically to the transmitted signal. The error sources due to the wireless channel are:

- Signal attenuation or path losses
- Multipath or Non-Line of Sight (NLOS) propagation
- Noise
- Narrowband and wideband interference
- Fading

The signal attenuation or path losses in 5G are higher because of the higher frequencies that are used with the mmWaves. The atmospheric absorption and the rain attenuation are also higher, but the short links that will be implemented overcome those effects. The material absorption will be also much higher with the mmWaves than with the current waves, also for the higher frequency that is used [11].

The multipath is the most common factor inside the wireless environment category. The multipath consists of having different paths to reach the receiver. As the authors indicate in [78], there is a possibility to maximize the throughput and minimize the latency by sending the data via different paths, increasing also the available bandwidth.

There is significant amount of available literature talking about how to solve the multipath problem, or how to use it for the user's benefit. Some examples of how to use the multipath in the positioning system are the algorithms Simultaneous Target And Multipath Positioning (STAMP) [46], Multipath-assisted Indoor Navigation and Tracking (MINT) [50], Multiple Signal Classification (MUSIC) [79], the EULOSTECH mitigation algorithm [80], and other NLOS mitigation algorithms shown in [79]: Weighted Least-Squares, Residual Weighting Algorithm, and Constrained Location. Also, solutions for different applications such as vehicle positioning [49], and assisted living [48] have been addressed.

The noise and the interferences disturb the positioning signals. The interference power will depend on the cross-correlation properties of the signals that are used. Regarding the noise, this acts as a jitter of the estimations that are done, e.g., in TOA and TDOA, the noise will act as a jitter of the estimated time of reception [21].

The geometric error sources are related to the physical parameters of the BS, such as the physical location, i.e., the coordinates, the geometry, and the size of his cell, as well as to the beamforming parameters in MIMO systems. Positioning performance is typically different when the BS is in one or another of the following environments: remote, rural, suburban, urban, indoor or underground [34]. The deployment of the BSs, which depends on the mobile operators, affects also to the positioning system, as it is mentioned in [32]. It has to be considered that the operators so far have not considered economically viable to invest in positioning, when the benefits are not going to be that high than the ones obtained from the communication. Nevertheless, this may change with the advent of 5G systems.

Examples regarding the computation and measurement error sources are clocks and the limitations of the hardware and/or software. Inside this error source group, the most critical source is the clock bias between the network nodes and MT.

Nodes and MTs are each equipped with an oscillator, and the internal clock reference is derived from this oscillator. This internal clock will be used to measure the "true" time. Because of some physical effects, the oscillators suffer from independent frequency drift. This small frequency drifts result in large timing errors [47]. To overcome with the clock synchronization errors, Kalman filters (KF) and extended Kalman filters (EKF), have been proposed to estimate the clock offset and this way minimize the position error [51].

Table 5summarizes the error categories that affect the positioning accuracy in a cellular system.

Error category	Error sources	Typical error magnitude
Wireless environment	Multipath propagation	few meters to few tens of meters
	Interference	few meters to few tens of meters
	Noise	few meters
	Fading	few meters
	NLOS propagation	few meters to few tens of meters
Geometric	BS location (coordinates)	few tens of meters
	BS geometry	few meters
	Cell Size	Few meters
Computation and measurement	Clock synchronization	few meters to few tens of meters
	HW limitation	few meters to few tens of meters
	SW limitation	few meters to few tens of meters

Table 5: Accuracy error categories and error sources

5. JOINT POSITIONIG AND COMMUNICATION ARCHITECTURES

This chapter reviews the state-of-the-art related to the joint communication and positioning system. If we consider OFDM signals, it is rather complicated to define an optimal waveform for both positioning and communication purposes. In the literature, several designs have been done showing for example that the optimal design in term of the RMSE, is the use of equi-spaced, equi-powered pilots [55].

5.1 Aspects of the joint positioning and communication architectures

The main aspects to consider in a joint positioning-communication architecture are:

- the design of the optimal transmission waveforms both for signaling and traffic transmission purposes
- the tradeoff between signaling overhead for positioning and the communication throughputs (optimal data-pilot allocation)
- the low-cost highly efficient architectures

In [54], the evaluation of the positioning capabilities is analyzed in realistic navigation channels. It is mentioned that many channel models have been defined and used widely for 5G system modeling. Some examples of these channel models are: Extended Pedestrian A (EPA) [54], [81], Extended Vehicular A (EVA) [54], [82], Extended Typical Urban (ETU) [54], [81], and Wireless World Initiative New Radio (WINNER) [54], [84], But the problem of these channel models is that they have been designed mainly for the communication system. This means that in these channel models, the time-delay offset between the BS and MT is not considered, and thus, there is no consideration of the bias introduced in the NLOS scenarios. New channel models have been developed [54], [83].

The Joint Maximum Likelihood (JML) time-delay and channel estimation is analyzed in [55] for OFDM signals. For that, in the same way that it has been used in this thesis, the matched filter is used as the maximum likelihood estimator, see section 6.4. But in real scenarios, the multipath need also to be considered. The introduction of the reflected or NLOS signals has a big influence in the estimator, because of the delays of these reflected signals, the bias of the estimator becomes bigger.

Similar JML solutions as the ones on [55] have been implemented before, e.g., see [85] and [86], but were mainly designed for the communication system. The problem resides in that for communications, there is no need for a very accurate time-delay estimation. To solve the multipath effect, a hybrid estimation model is proposed in [55], where equi-spaced taps are used with an arbitrary tap between the first two. By the introduction of one more estimation parameter, i the characterization of the channel is improved, and this helps to increase the positioning accuracy in multipath environments.

A similar study to the one done in [55] was achieved in [60] where the authors proposed a unified framework which solves the time synchronization and localization problems jointly in a wireless sensor network.

Other studies mention the problems with the MT oscillator, which affect to the TOA estimation method. So, the authors in [51] proposed to use an extended Kalman filter (EKF) to improve both user position and the clock offset. In order to increase even more the user position estimation, the TOA is combined with the DOA estimation method. The conclusions were that the 5G is indeed able to reach the sub-meter accuracy range estimation, and that the joint DOA/TOA-EKF outperforms the existing DOA-only solutions, while obtaining a high accuracy in the MT clock offset estimation.

In [58], the authors proposed a model for channel variability of different OFDM symbols by varying, for a given channel power, the channel mean and the covariance. The effect of channel variability is investigated in the joint design of pilot and data power allocation. The results obtained from the investigation showed that for a given channel power, if the channel covariance is reduced and the channel mean is increased, the accuracy of the estimation of both the channel parameters and the time-delay is improved. They also proved that with this method, the channel capacity increases. So, the authors concluded that in an OFDM system with correlated OFDM symbols, the information from previous symbols can be used to improve the estimation accuracy and SINR.

When OFDM signals are wanted to be used for joint communication and positioning, there is a challenge in finding the optimal data and pilot power allocations. In [59], the authors propose an optimization problem, and use asymptotic bounds to reduce the computational complexity of the optimization problem. In consequence, the number of subcarriers and channel taps is increased. The conclusion reached in this investigation is that the performance of joint communication and positioning is negligibly affected. Also, it has been proven that the asymptotic bounds converge to the non-asymptotic bounds after certain number of subcarriers.

The typical channel models are the single-tap model [54] , arbitrary-tap model [54], and periodic tap model [54], described in the next section.

5.2 Channel models

The **single-tap model** is the simplest and most used channel estimation model [54]. It only adds attenuation and delay to the propagated signals. This is the one used in this thesis to develop the indoor channel model. The added delay will depend on the sampling time of the transmitted signal, and is calculated with the expression (20), where t_ϵ is the propagation delay, and T_s is the sampling time of the transmitted signal.

$$\tau = t_\epsilon / T_s \text{ [samples]} \qquad \textbf{(20)}$$

With single-tap channel models, a matched filter or a correlation-based estimator provides the optimal performance in the maximum likelihood sense. But in multipath environment with high delay spread, it may not be appropriate to apply this kind of channel models [54].

The **arbitrary-tap model** is the most accurate model due to the fact of estimating the amplitude, phase, and delay of every physical ray of the multipath channel. This fact makes it also the most complex model, but also the most realistic channel model compared with the other three. The implementation complexity is one of the biggest concerns [54].

The **periodic-tap model** reduces the complexity of the channel estimation by placing the estimation taps in a periodic delay positions. The estimation taps can also be in equispaced position. The purpose of placing the taps is to focus on the propagation time-delay of the signal. This avoids the delay calculation of each physical ray. Thus, the channel model is less realistic than the arbitrary-tap model, but much simpler. By using this method, the resulting model is a sampled version of the channel impulse response.

The most used channel model for the 5G system are the one created by METIS, which will be explained in the Section 7.1, and WINNER II [87]. One of the advantages of the WINNER II channel model is that it is possible to use it for different environments. It is able to model indoor channels, indoor to outdoor channels, and outdoor channels. Regarding to the positioning, WINNER II allows to know the departure and arriving angles, the received power and the propagation delay [87]. An extension of the WINNER II channel model is Quadriga, which can be used for the terrestrial and satellite communications [87].

6. SIMULATION ENVIRONMENT: WAVEFORMS

In this chapter, the simulation environment will be explained regarding to the waveforms used. Our model started from the initial Matlab software package provided by our colleague at ELT, Dr. Jukka Talvitie and Dr. Toni Levanen. As this model is one of the core elements of the simulations used in this thesis, the implementation of the three 5G studied waveforms will be explained in this chapter. In the chapter 7, also the Matlab channel models and the developed Graphical User Interface (GUI) will be explained.

During this project, three waveforms have been used: WCP-COQAM [12], [15], ZT-DFT-s-OFDMA [13]-[15], [71], and CP-OFDMA [15], [16], [71]. These three waveforms have been selected for been an improvement of (or been used in) the current 4G waveforms, or because of their advantage over the OFDM, the case of WCP-COQAM [88].

6.1 Block diagram of the 5G waveforms

In this section, several 5G waveforms will be explained with the help of block diagrams. The waveforms that will be analyzed are: ZT-DFT-s-OFDMA, CP-OFDMA, and WCP-COQAM.

The first waveform to be analyzed is CP-OFDMA, and its block diagram is shown in Figure 4. The information bits are the input of the transmitter. These are modulated and the constellation is converted from serial parallel. Having the information in parallel, the IFFT is applied, after that, the cyclic prefix (CP) samples are added and the output of this operation is the CP-OFDMA waveform. This is the block diagram of a classical OFDM signal [88], [89].

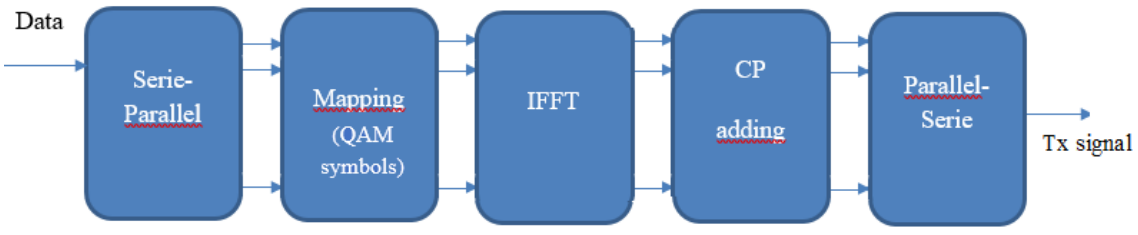

Figure 4: CP-OFDMA transmitter block diagram

The second waveform to be analyzed is ZT-DFT-s-OFDMA. The method consists in the Discrete Fourier Transform (DFT) that is applied after modulating the incoming bit stream. Once the DFT, a predefined number of zeros are added at the beginning and in

the tail of the signal to be transmitted. After that, the IFFT is applied and the signal to be transmitted is obtained. The full block diagram can be seen in Figure 5.

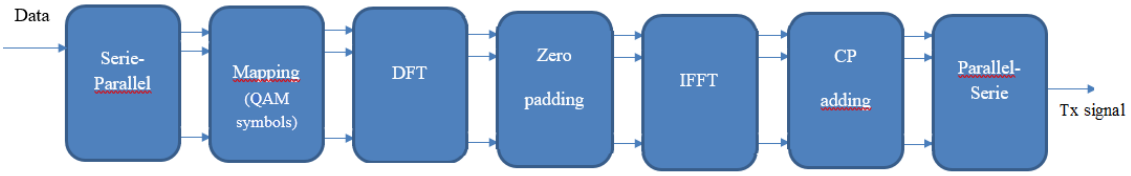

Figure 5: ZT-DFT-s-OFDMA transmitter block diagram

The WCP-COQAM signal transmitter can be seen in Figure 6. The main difference between this waveform and the previous ones is that after the QAM modulation, this is converted to the OQAM baseband signal, in the QAM/OQAM conversion block in Figure 6. During this conversion, OQAM uses a linear convolution, but if a circular convolution is applied instead, the result will be a COQAM modulation. When switching the linear convolution for a circular one, the COQAM modulation gets rid of the drawbacks of OQAM, while keeping almost all the benefits [88]. Once the COQAM signal is obtained, it is prepared for the transmission, applying a windowing after the CP is introduced.

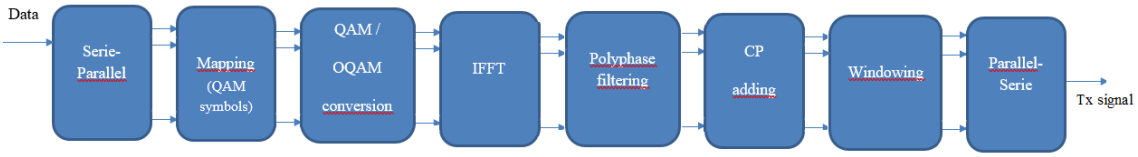

Figure 6: WCP-COQAM transmitter block diagram

6.2 Mathematical models

In this section, the mathematical models are shown for the implementation of the different waveforms that are used during the thesis.

First of all, the CP-OFDMA and ZP-DFT-s-OFDMA waveforms are defined. To generate these waveform, a basic OFDMA waveform is need to be implemented. This expression is given in (21).

$$s_{OFDM}[k] = \sum_{m=0}^{M-1} c_m e^{\frac{j2\pi mk}{M}} \qquad \textbf{(21)}$$

where $M$is the number of subcarriers and c_m the complex valued data symbols. Once the OFDMA waveform is generated, the corresponding proceedings shown in the section 6.1 are applied to obtain the corresponding waveform.

Once the OFDMA waveform is obtained, the cyclic prefix (CP) is added, obtaining the following expression:

$$s_{CP-OFDM} = \begin{matrix}[s_{OFDM}[M-G], s_{OFDM}[M-G+1], \dots s_{OFDM}[M-1], s_{OFDM}[0], \dots^{T} \\ s_{OFDM}[M-1] \dots]\end{matrix} \quad \textbf{(22)}$$

where *M* is the number of subcarriers, and *G* the length of the cyclic prefix.

The analytical expression of the ZT-DFT-s-OFDM signal is provided in (23).

$$r_{ZT-DFT-s-OFDMA}[k] = \frac{1}{\sqrt{M_{IFFT}(M-M_t-M_h)}} \boldsymbol{F} \cdot \boldsymbol{T} \cdot \boldsymbol{D} \cdot x \quad \textbf{(23)}$$

where x_k is the vector with the modulated symbols, $\boldsymbol{D}$ is a matrix that performs the DFT operation, $\boldsymbol{T}$ is the mapping matrix for subcarrier assignment, and $\boldsymbol{F}$ performs an M_{IFFT} points IFFT operation. The M_{IFFT} parameters represents the number of points used in the IFFT operation, and M_t and M_h are the number of zero valued symbols added in the tail and head, respectively.

In order to generate a WCP-COQAM waveform, the first step is to generate a COQAM signal, which baseband expression is given below.

$$s_{OQAM}[k] = \sum_{m=0}^{M-1} \sum_{n \in Z} a_{m,n}\, g[k-nN_1] e^{j\frac{2\pi}{M}m(k-\frac{D}{2})} e^{j\Phi_{m,n}} \quad \textbf{(24)}$$

where g is the prototype filter, and is assumed to be real-valued and symmetrical; M is the number of subcarriers; $N_1 = M/2$ is the discrete-time offset; $\Phi_{m,n}$ is an additional phase term at subcarrier m and symbol index n which can be expressed as $\frac{\pi}{2}(n+m)$. In the Matlab simulation, the design of the filter prototype is the first operation. Before obtaining the symbol map, the bits are grouped and the modulation takes place. The available modulations are 4QAM, 16QAM, and 64QAM.

Once the OQAM symbols are obtained, the cyclic convolution is applied, as mentioned in the section 6.1. Analytically the COQAM symbols can be calculated with the expression (25).

$$s_{COQAM}[k] = \sum_{m=0}^{M-1} \sum_{n=0}^{K'-1} a_{m,n}\, g[k-nN_1] e^{j\frac{2\pi}{M}m(k-\frac{D}{2})} e^{j\Phi_{m,n}} \quad \textbf{(25)}$$

where *K'* is the number of real symbol slots per each block.

So, the WCP-COQAM expression is obtained after the adding the CP and the windowing. The analytical expression of WCP-COQAM is shown below.

$$s_{WCP-COQAM}[k] = \sum_{r=l-1}^{l+1} s_{COQAM}[\mathrm{mod}(k - L_{CP}, MK)] \quad \textbf{(26)}$$

where L_{CP} is the length of the CP and l is the block index.

6.3 Building the simulator

The simulator that is implemented in this thesis is based on a transmitter, a receiver, and two channel models. The channel models will be explained in detail in the Chapter 7. A block diagram of the simulator and an explanation of its behavior is given in the section 6.3.1. The different parameters that are needed to run the simulation are explained in the section 6.3.2.

6.3.1 Block diagram

In Figure 7 the block diagram of the developed simulator is shown. The transmitter is composed by three main blocks, the waveform generator, where the three waveforms used within this thesis are generated. From this block, the signal to be transmitted is obtained. The signal is oversampled, and then shaped with the Squared Root Rise Cosine (SRRC).

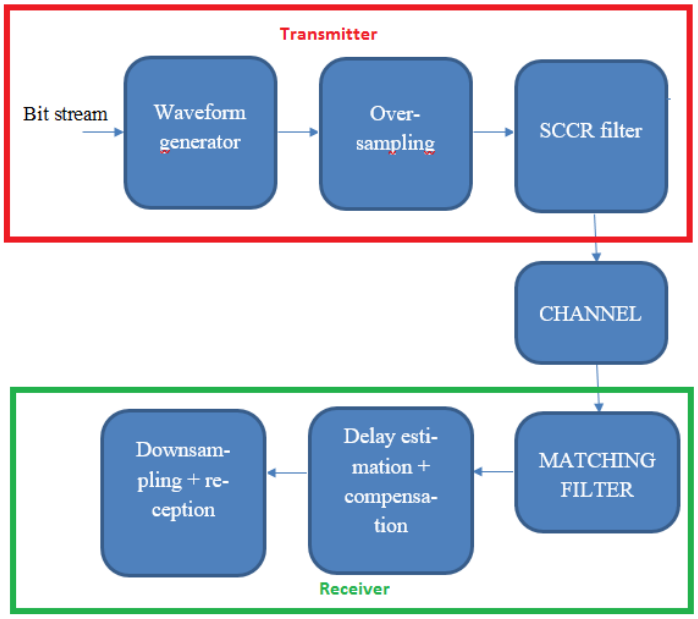

Figure 7: Block diagram of the simulation

The output of the SRRC, is the transmitted signal, which is used in one of the two channel models explained in Chapter 7.

The receptor consists in a matched SRRC filter, that filters the signal as soon as it is received. After the filtering, the channel delay is estimated and compensated, this pro-

cedure is explained in section 6.4. After that, the downsampling is implemented, obtaining the same sample frequency than the one obtained at the output of the waveform generator. Finally, the signal reception is implemented, and the evaluation of the QoS is implemented.

Part of this thesis is related to the distance estimation, and this has been achieved by incorporating the distance-based channel delay model in the simulator. In order to obtain a better time-delay accuracy, the sampling frequency of the signals obtained in the previous section, has been increased 25.08kHz to 1.25MHz. To increase the sampling frequency, an oversampling factor was defined. The oversampling factor obtained in this thesis has been limited to 50, i.e., per each signal sample, 50 new samples have been added. This decision was taken due to the long simulation times and the insufficient computing resources. In actual systems, a higher sampling frequency than the one used in this thesis is used, but this will be discussed in the chapter 8.

With an oversampling factor of 50, an accuracy of around 120m is achieved with the three waveforms. Each one of the waveforms has a different sample length, making them have different accuracy level. As shown in (20), the bigger the number of samples contained in the generated waveform, the bigger the number of samples to add in the channel delay modeling. As it is mentioned in [57], a sampling frequency of 153.6MHz is proposed to achieve the 1m accuracy, what is translated in an oversampling factor close to 6000 in the developed simulator.

The simulations with such a high oversampling factor, namely 6000, require a huge computational load, and it takes long time to make the calculations for one iteration. So, in order to obtain fast and significant results, and considering that for each measurement 50 independent realizations are performed, an oversampling factor of 50 has been chosen. Table 6 shows the achievable positioning accuracy that is related to each oversampling factor.

Oversampling factor [samples]	**Achievable positioning accuracy [m]**
50	120
100	60
500	12
1000	6
6000	1

Table 6: achievable positioning accuracy for different oversampling factors

The oversampling process requires a pulse shape filter. In this thesis, a square raise root cosine (SRRC) filter has been defined for shaping the oversampled signal. At the receiver side, the received signal is again filtered with a matched filter, namely another SRRC filter. After that, the delay estimation will be applied, based on the Maximum Likelihood theory, as shown in (27).

$$\hat{\tau} = \arg\max_{\tau}\{\left|R_{yx}(\tau)\right|^2\} \quad \textbf{(27)}$$

where $R_{yx}(\tau)$ is the correlation function between the transmitted signal and the received signal after the matching filter [54]. Considering that the signals have the cyclic prefix, they introduce a circular symmetry in the signal at the output of the channel. The correlation between the transmitted signal and the received one is defined in (28).

$$R_{yx}(\tau) = \sum_{m=0}^{N-1} y(m) \cdot x_s^*(m-\tau), \quad \textbf{(28)}$$

where $x_s^*(m)$ is a circular shifted and conjugate version of the original $x(m)$. This operation will return the number of estimated delayed samples, which can be converted into the estimated distance. Before converting the estimated delay samples into the distance, the SRRC filter delays have also to be taken into account and removed.

6.3.2 Simulation parameters

Before generating any waveform, there are some general parameters that need to be defined, such as the number of independent data realization, which will be used in order to obtain representative results. In the Table 7, the general parameters that are not directly related with the waveform design are shown.

Parameter name	**Parameter description**	Parameter values
maxIndependentDataRealizations	number of independent realizations	100
modelPAEffect	indicates if the power amplifier is modeled in the transmitter	True/false
modelWindowedClipping	indicates if the windowed clipping is used with power amplifier modeling	True/false
channelModel*	defines the channel model to be used.	'*unityChannel'*
SNRVector**	values of the snr to be used during the simulation	From -20 to 30
modulation	the modulation to be used in the simulation	4QAM/16QAM/64QAM
bitsPerSymbol	the number of bits per symbol. It is linked to the modulation	2/4/6

* not used in this project
**only used in BER measurements

Table 7: General simulation parameters

In the simulations, the used channel model is the *"unityChannel"*, which is the ideal channel, a delta with a weight of 1. The main reason of using this channel is that the channel models that are used in this thesis are not defined in within these files, are external. Thus, there will not be any overlapping between this channel model and the ones defines in Chapter 7.

More general parameters are shown in Table 8, and they are related to the waveform design, with OFDM waveforms to be more precise.

Parameter name	Parameter description	Parameter values
nbrSubchannels (M)	number of subchannels	2048
nbrMCSymbols	number of multicarrier symbols in the block	12
CPChannelLen	length of the cyclic prefix that is used to fight the channel interference	115
CPWindowLen	length of the cyclic prefix used for windowing	0
CPLen	total length of the cyclic prefix. It is calculated with the following expression: $CPChannelLen + CPWindowLen$	115
CPGenerationOption	indicates the algorithm for generating the cyclic prefix	1: copies the CP length number of samples from the end to the beginning 2: copies the CPChannel-Len+CPWindowLen/2 number of samples form the end to the beginning and CPWindowLen/2 from the beginning to the end 3: the contrary operation of the option 2.
waveformType	indicates the waveform to be generated	'OFDMA' 'OQAM' 'DFT-s-OFDMA'
nbrSCPerRB	number of active subchannels per resource block	160
nbrRBs	number of resource block	8
activeRBs	number of active resourceblocks	Vector of ones and zeros of the length nbrRBs mentioning which resource blocks are active (1) or not (0).
nbrSCPerGB	number of subchannels acting as Guard Band	0

Table 8: General waveform parameters

In the Table 8, it is possible to see the general waveform parameters. With the parameters described here, the main information is obtained for the waveform design, e.g., the number of subchannels, the number of resource block, the number of subchannels per resource block, the length of the cyclic prefix, etc.

The cyclic prefix can be generated by different algorithms, and the use of each one will depend on the numerical value assigned to the parameter *CPGenerationOption*. The algorithm used in the simulations copies the same number of samples than the length of the cyclic prefix, which is the value of the parameter *CPLen*, from the end of the signal to the beginning.

In the Table 9**,** the specific parameters for the WCP-COQAM waveform design are shown. In the simulations, the parameters *useCircularAddition, windowSymbolBlock,* and *addSymbolBlockCP* will be activated, so the waveform used in the simulations is WCP-OQAM.

Parameter name	Parameter description	Parameter values
prototypeDesignOption	prototype to design the waveform	1->Nearly Perfect Reconstruction (NPR) filter bank 2->Perfect Reconstruction (PR) filter bank {3,1}-> Root Rise Cosine prototype filter with roll-off factor of 1 {4,1}->Rise Cosine prototype filter with roll-off factor of 1
overlapFactor	overlap factor used in the filter bank design	4
useCircularAddition	defines if circular addition is used in the signal construction. This will shorten the symbol block in time domain	True/false
addSymbolBlockCP	determines if a cyclic prefix is added to the symbol block	True/false
windowSymbolBlock	Determines if the symbol block is windowed	True/false
ReferenceSymbolDesign	Defines the reference symbol used for channel estimation	'QAM'

Table 9: WCP-COQAM waveform parameters

Table 10 shows the configuration parameters of the CP-OFDMA waveforms. For this waveform, it is possible to add a windowing and a cyclic-prefix.

Parameter name	Parameter description	Parameter values
useTxSignalWindowing	Indicates if the transmitted signal is windowed	True/false
useMCSymbolwiseWindowing	Indicates that each OFDM symbol is windowed	True/false
addSymbolwiseCP	Indicates if a cyclic prefix is added at the beginning of each symbol	True/false
useTxSignalFiltering	Indicates if the transmitted signal is filtered	True/false
UseMCSymbolwiseFiltering	Indicates if each OFDM symbol is filtered	True/false

Table 10: CP-OFDMA waveform parameters

Table 11 and Table 12 show the dedicated waveform parameters for the ZT-DFT-spread-OFDMA waveform.

Parameter name	Parameter description	Parameter values
addZTInDFTInput	indicates if there is a "Guard period" implemented between separate symbol (a zero-tail part of the multicarrier symbol).	True/false
ZTGPLength	length of the zero-tail guard period	90
nbrZerosHead	number of zeros subcarriers in the head of the DFT input	1
nbrZerosTail	Number of zero subcarriers in the tail of the DFT input	8
referenceSymbolDesign	Indicates the reference symbol design	'firstSymbol -Random': a randomly generated symbol place in the first symbol of the frame
channelEstimateFilter	channel estimator filter	'none'

Table 11: ZT-DFT-s-OFDM waveform parameters

Table 12 shows the parameters used for the spectrum analysis, i.e., the PDF of the transmitted and the received signal.

Parameter name	Parameter description	Parameter values
useFFTBasedAnalysis	indicates if the analysis is going to be based on the FFT	True/false
PSDFFTSize	FFT size used for evaluating the power spectral density (PDF)	2^(nextpow2(nbrSubchannels+8))
useFBBasedAnalysis	indicates if the analysis is going to be based on the filter banks	True/false
nbrSubbandInSpectrumAnalysis	number of subbands used in the spectrum analysis	512
outputInLog	indicates if the power spectral density is given in logarithmic scale	True/false
normalizePSDToUnity	normalizes the maximum component of the PSD into unity	True/false

Table 12: Parameters used in the spectrum analysis

6.4 Simulator performance criteria

The performance criteria that are evaluated in this thesis are the BER for the QoS of the communications and the CRLB and distance estimation error for the positioning accuracy.

6.4.1 BER

To compute the bit error rate, a wide range of SNR values have been used. To obtain the value of this parameter, the demodulated bits are compared with the bits that are going to be transmitted. Obtaining the percentage of the received bits with errors, the BER is calculated. This is evaluated for the three waveforms used in this thesis, and for different modulation orders, e.g., 4QAM, 16QAM, and 64QAM.

6.4.2 CRLB of distance error

The CRLB is measured also in a wide range of SNR conditions. Considering that it will give the lower achievable variance of the estimator that is being used in the thesis, it is expected to obtain low distance error values. To calculate the CRLB, the expression (16) is used. Considering that it is inversely proportional to the SNR, the value of the CRLB decreases when the SNR increases.

6.4.3 Distance estimation error

This will measure the real distance error produced by the distance estimation process. Following the expression (27), the distance estimation depends on the number of estimated delay samples. The number of estimated delay samples is multiplied by the sampling time and the speed of light, obtaining the estimated distance. Knowing the estimated distance and the real distance the distance error is computed.

As mentioned, the estimated distance depends on the sampling time, i.e., the sampling frequency. So, increasing the sampling frequency, it is possible to improve the accuracy of the estimator. The relation between the sampling frequency and the achievable positioning accuracy is given in Table 6.

The simulation results are shown in Chapter 8.

7. SIMULATION ENVIRONMENT: CHANNEL MODEL AND GUI

In this chapter, the channel models and the GUI built in the thesis will be explained. Two channel models have been used, one for the outdoor environments, and another one for indoor scenarios. For the outdoor channel model, the starting point has been the METIS 5G channel model. For the indoor channel model, a simple indoor channel model based on a multi-floor building map has been developed. While the outdoor channel model supports multi-link configurations, the indoor channel model supports only single-link configurations. The map used for indoor channel model is based on the map of one of the buildings at Tampere University of Technology (TUT).

7.1 Outdoor channel model

The starting point of the outdoor channel model used in this thesis has been the 5G channel model developed in the European METIS project [53]. This channel model consists of rectangular buildings, with predefined width and height. The buildings do not need to have the same height, i.e., two building next to each other can have different height. The widths of the buildings and of the streets, however, are fixed and constant.

The number of buildings in the scenario can also be configured. Considering that the scenario will involve a square area, the user will have the chance of defining the number of building in the X axis and in the Y axis. The Figure 8 a) shows an example of the METIS channel model in 2D, and the Figure 8 b) shows the same scenario but in 3D.

The outdoor channel model is in 3D, thus the power map is measured at different heights, i.e., inside a building, per each floor one measurement will be done for a fixed (*x*,*y*) coordinate. If the measurement point is outside a building, its maximum height will be limited to 0 (ground level). The maximum height is thus defined in (29) .

$$Z_{max}(x,y) = \begin{cases} 0 & if\ x,y\ in\ the\ street \\ height\ of\ the\ building & if\ x,y\ inside\ a\ building \end{cases} \quad \textbf{(29)}$$

In (29), the height is represented in function of the values in the *X* and *Y* axis because they are used to determine if the measurement point is inside a building or outside.

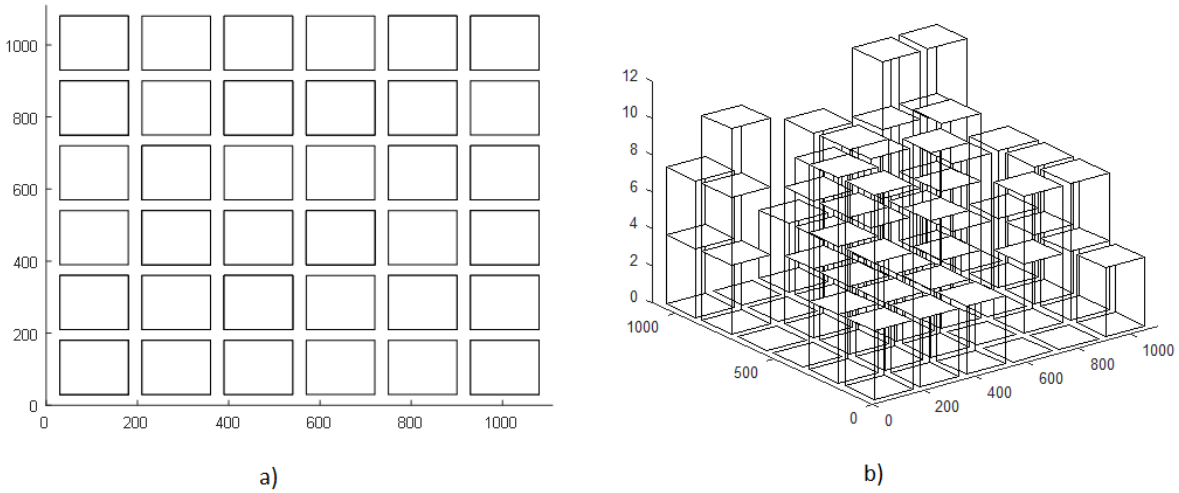

Figure 8 .a) 2D view of the METIS channel model, b) 3D view of the METIS channel model

The amount of the measurement points will depend on the resolution introduced previously by the user. This resolution will divide the area map in squares of same lengths in meters, i.e., if the value of the chosen resolution is 2, the resolution cell will be 2m x 2m.

The next step is to define the limits of the street, i.e., the x and y axis positions representing the street. This information is used to randomly locate the transmitter and the receiver in the street, i.e., it is not desired to locate them inside a building, as for that kind of measurements the indoor channel model has been developed. Once the transmitter and receiver are located, the channel model will start to make the measurements.

For that, first the exact location of the BS is needed, and for that, the channel model will check every horizontal and vertical street[2] to check where the BS is. Once checked if the BS is in a vertical, horizontal, or intersection, the same procedure starts with the measurement points. All the measurement points of the map are analyzed in order to calculate the power received in those points.

For that, first the street in which they are located is calculated, using the same methodology that is used for searching the street of the BS. After that, the straight line between the transmitter and the measurement point is calculated. Once the direction is known, the next step is to check if the transmitter and receiver are in a LOS path. If so, the path loss for that point is directly calculated, by means of the following path loss expression [2].

[2] If the Figure 8 a) is checked, the horizontal streets will be those with fixed y coordinates, i.e., those starting in the left and finishing on the right. The vertical streets, however, will be those with fixed x coordinates, i.e., those going form up to down.

$$Llos = 40\log_{10}(d) + 7.8 - 18\log_{10}(htx_{eff}) - 18\log_{10}(hrx_{eff}) + 2\log_{10}(f/1GHz) \quad \textbf{(30)}$$

where d is the distance difference between the measurement point and the center of the street; htx_{eff} and hrx_{eff} are effective antenna heights of the transmitter and the receiver, respectively, and *f* is the carrier frequency in GHz.

If the transmitter and the receiver are not in a LOS path, it is checked if the receiver is in a perpendicular or parallel street. If the receiver is in a parallel street, it is considered that the received signal is below the functionality threshold of the receiver.

However, if the transmitter is in a perpendicular street, the receiver is in NLOS, so a new expression must be used [53].

$$PL(d1, d2) = Llos(d_1) + 17.9 - 12.5\,n_j + 10n_j\log_{10}(d_2) + 3\log_{10}(\frac{f}{1GHz}) \quad \textbf{(31)}$$

where d_1 and d_2 are the distances from the BS and MT to a cross section of the street, respectively. The parameter n_j is calculated by the expression (32).

$$n_j = \max(2.8 - 0.0024d_1, 1.84). \quad \textbf{(32)}$$

The value that will be saved in the measurement matrix will always be the maximum value between the calculated path loss and the minimum coupling loss (MCL). The MCL will be also introduced by the user. In the thesis we chose, 0,

This method is also used to estimate the received power in indoor environments. More information about this channel model can be found in the literature [53].

7.2 Indoor channel model

This a simple channel model designed for indoor environments. This channel model, which is also implemented in MATLAB, is based in a building of TUT. An example of the map of the building can be seen in the Figure 9.

The positions of the transmitter and the receiver are placed randomly inside the building walls.

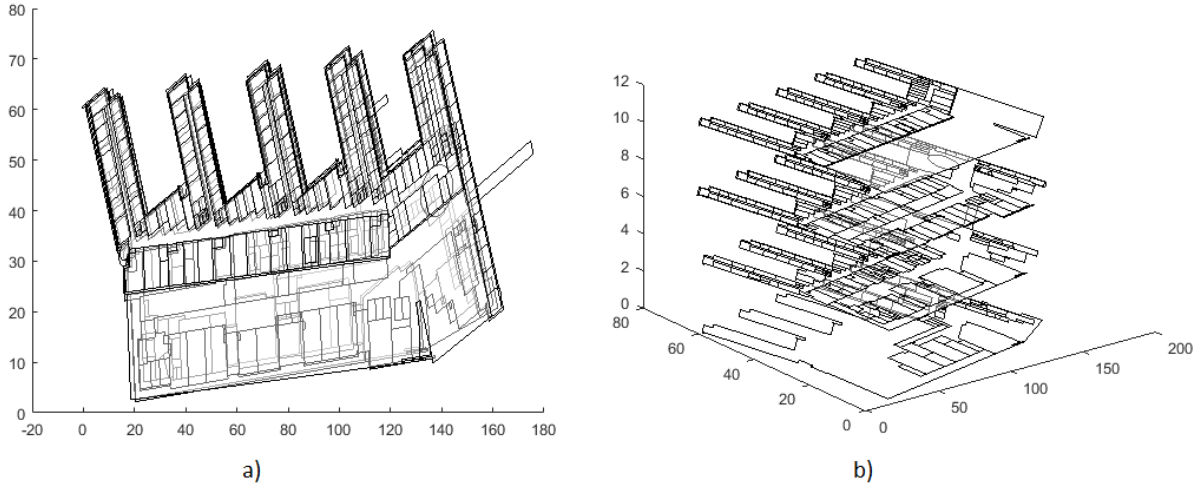

Figure 9. a) TUT university building, floor view (2D) for the indoor channel model b) TUT university building, 3D view for the indoor channel model

The next step is to calculate the received power in each of the MT locations, based on the corresponding BS. For this, a simplified path loss model has been implemented, where the path loss depends on the distance *d* and on a path loss parameter *n* only.

$$L_p = 10\, n\, \log_{10} d, \tag{33}$$

where n is the path loss exponent, and d is the distance between the transmitter and the receiver. To this propagation loss other effects are added, such as the loss due to the indoor walls, outdoor walls, or the losses due to the floor. The attenuation of each one of these effects, are introduced previously by the user.

The losses due to the indoor walls are computed with an approximation. With the map of the building of TUT, the corners of the rooms have been provided. To compute the number of walls that a signal crosses inside the building, an estimation is done, in which the distance between the transmitter and the receiver, and the average length of the room are considered. First, the rooms are assumed to be squared, and thus, the average distance of the room is computed by applying the square mean root to the average area of all the rooms of the building. After that, the distance between the transmitter and the receiver is calculated in the X and Y plane only. Dividing this distance by the average distance of the room, the average number of indoor walls that the signal crosses is estimated. Knowing the number of indoor walls and the losses that each indoor wall induces to the signal, the total losses caused by the indoor walls are calculated.

For the total losses caused by the outdoor walls, it is checked if the transmitter and the receiver are inside the building. This loss is applied only if the transmitter is inside the building and the receiver outside, and vice versa. The losses caused by the outdoor walls are introduced by the user.

The floor losses are applied only in the cases in which the transmitter and the receiver are in different floor of the building. In this case, the height of the user and receiver are used. It is checked each one in which floor they are located and the difference of the floors will give the value of the floor difference between the transmitter and the receiver. The losses caused by the floor are also introduced by the user.

The shadowing effect has been implemented as a variable that follows a Gaussian distribution, and with a variance introduced by the user. The total losses are finally computed with the expression in (34).

$$L_{TOT} = L_p + n_{iw} \cdot L_{1,iw} + n_{ow} \cdot L_{1,ow} + n_{fl} \cdot L_{1,fl} + \Psi_f(0, \sigma_f^2) \quad \textbf{(34)}$$

where n_{fl}, n_{iw} and n_{ow} are the number of floor, indoor walls, and outdoor walls that crosses the transmitted signal, respectively, , $L_{1,fl}$, $L_{1,iw}$ and $L_{1,ow}$ are the losses caused by one floor, one indoor wall, and one outdoor wall, respectively, and $\Psi_f(0, \sigma_f^2)$ is the losses caused by the fading, that follows a Gaussian distribution with 0 mean value and with a variance σ_f^2, which will be introduced by the user. The losses of one floor, one indoor wall, and one outdoor wall are also introduced by the user, at the beginning of the simulation.

7.3 GUI

The developed graphical user interfaces within this thesis are simple interfaces that will help the user to introduce the requested parameters, which will be needed to run the simulations. Some examples of these parameters are: carrier frequency, the transmitted power, noise power spectrum density (N_0), and the number of users *N*.

When running the simulation, three graphical interfaces will be shown: one will allow the user to choose between the outdoor channel model and the indoor channel model, the second one will allow the user to introduce the values of the indoor parameters, and the third one allows the user to introduce the values of the outdoor parameters.

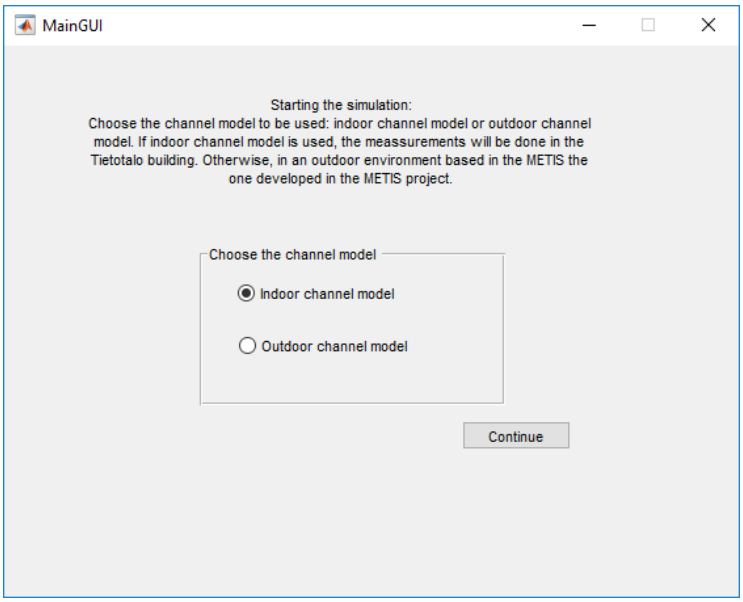

Figure 10: Initial GUI window

Once channel model type is selected, the GUI related with the corresponding channel model will be shown. In Figure 11 the GUI for the indoor channel model is shown. By this GUI, the user is requested to introduce all the information related to the losses due to the walls and ground. Also, the value for the noise power spectral density, the carrier frequency, and the transmitted power, as mentioned before in section 7.2.

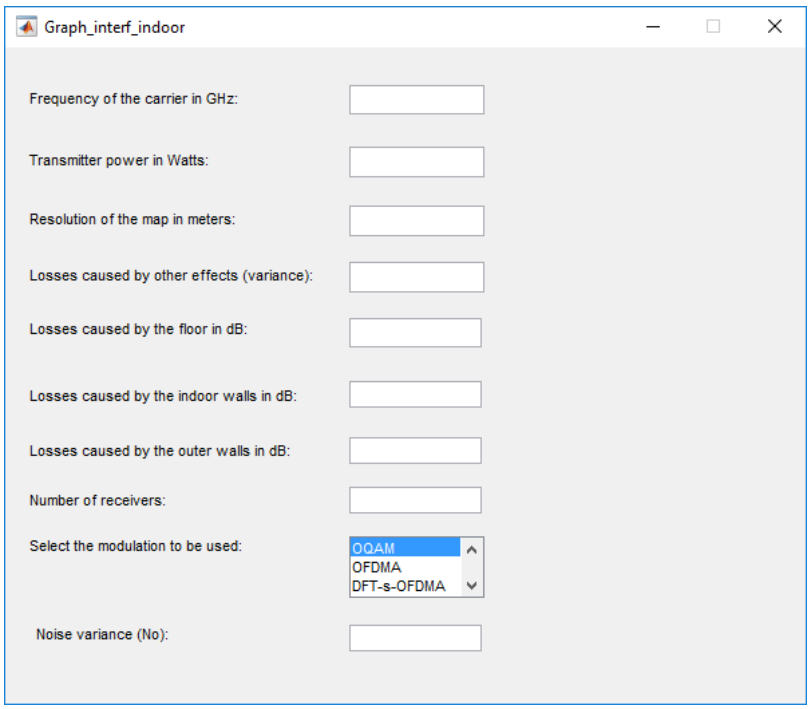

Figure 11: Indoor channel model GUI

In the Figure 12 the GUI for the outdoor channel model is shown. Among the information requested to the user, we can see some of the initial parameters mentioned in

7.1: the carrier frequency, the transmitter power, the number of buildings in the x axis and y axis, the resolution of the map, and the width of the street and the building.

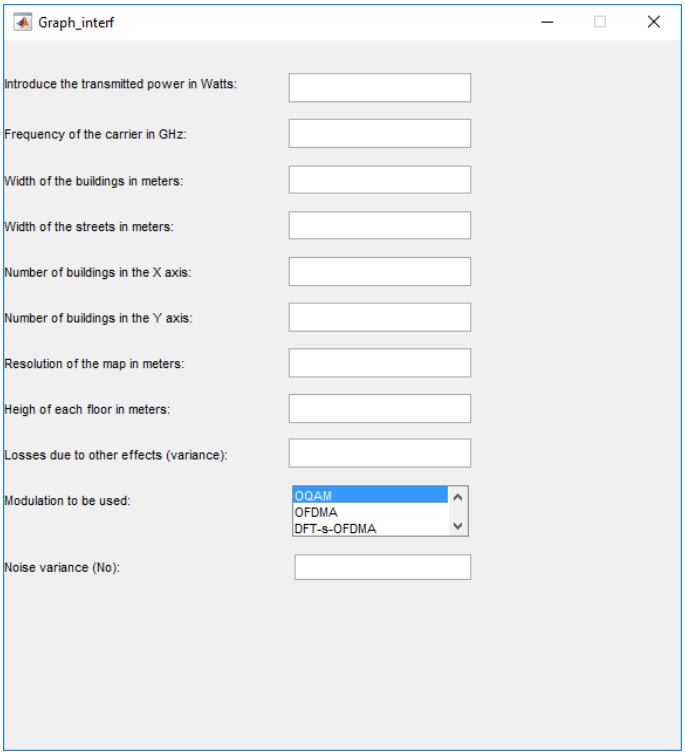

Figure 12: Outdoor channel model GUI

In the following chapter, the simulation set-up and the results of the simulations are shown.

8. SIMULATION RESULTS

This chapter focuses on the simulation results. The obtained simulations include three main aspects: the coverage, the distance estimation error, and the QoS of the communications. The coverage area is shown by means of a power map, where the received power is shown in the different places of the map. The distance estimation error is evaluated based on 3 different 5G waveforms by the means of the CRLB. Finally, the QoS is analyzed in terms of BER.

In our simulations, the number of random data realizations has been set to 50 and the oversampling factor was set up to 50.

8.1 Coverage areas

First the coverage areas have been analyzed in the outdoor channel model. The results can be seen in Figure 13 for both 2D (left figure) and 3D (right figure) models. In these figures is possible to notice one red and one green point, which represent the transmitter and receiver, respectively. In both cases, the received power in all the points of the map is shown. The white zones mean that the received signal power is lower than the threshold, which has been stablished to -100dBm, based on the typical sensitivity of a receiver [add refs that talk about 5G rx sensitivity]. This means that if the received signal power is lower than -100dBm, we assumed that the MT is not able to detect the signal.

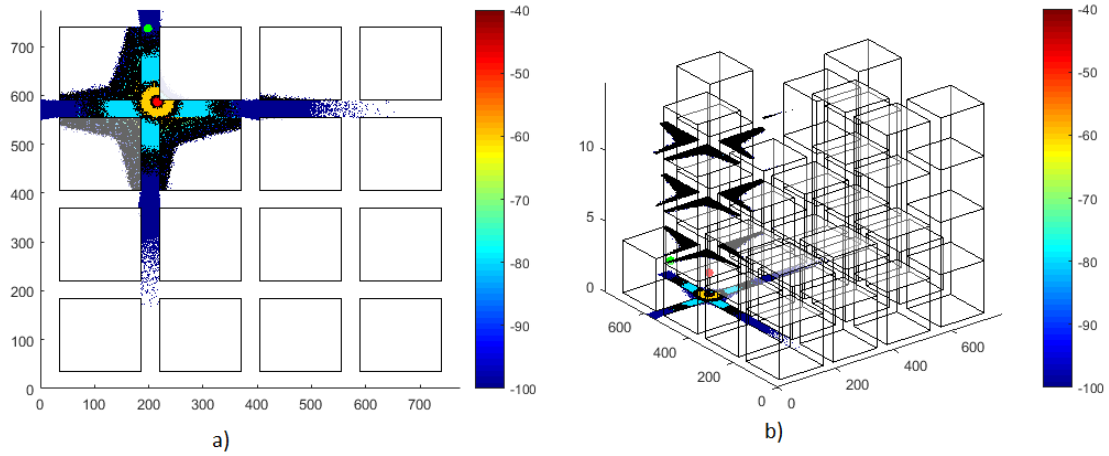

Figure 13. a) Outdoor channel model power map in 2D; b) Outdoor channel model power map in 3D

The network configuration used for achieving this result is shown in Figure 14: transmission power of 1W, or equivalently 30dBm, and a carrier frequency of 10GHz, i.e.,

inside the mmWave band. In the used configuration, the buildings are 150m wide and the height of the buildings, i.e., the number of floors is randomly assigned from 1 to 4, having a floor height of 3.7m. The chosen map size was not big, only 4 buildings in the x axis and another 4 in the y axis, making a total of 16 buildings in the deployed map for a clearer illustration. A resolution map of 1m x 1m has been chosen to make the power reception calculations.

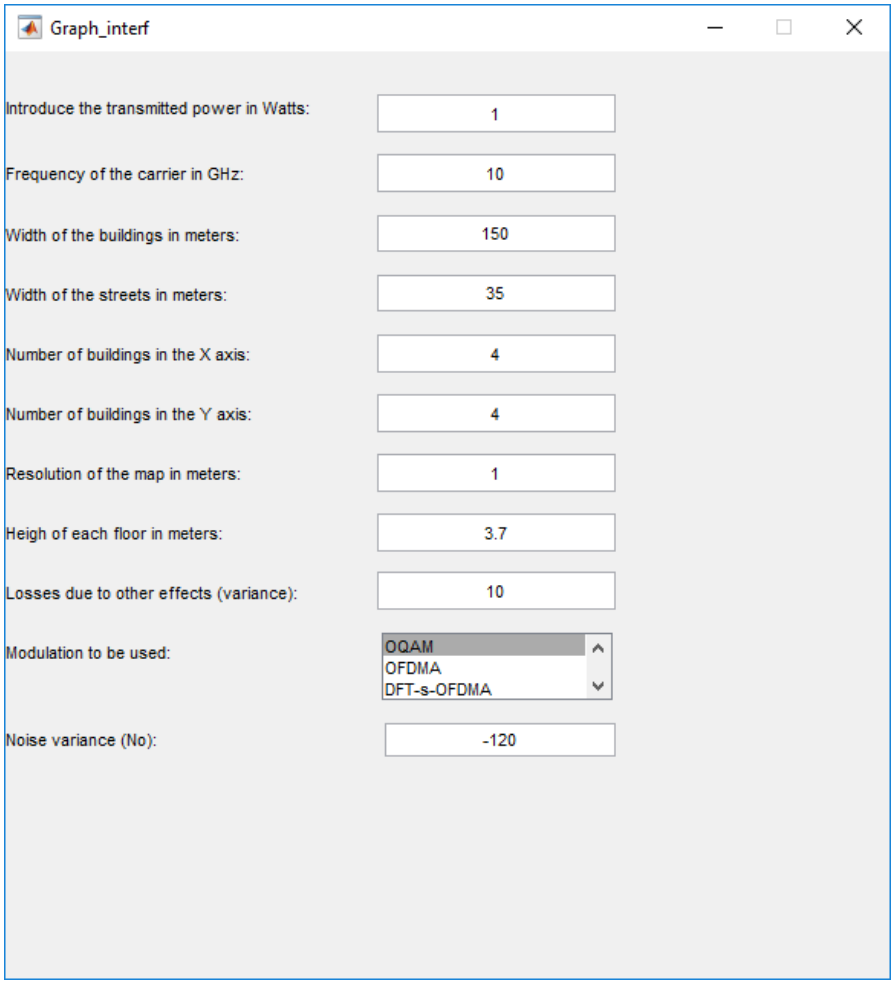

Figure 14: Network configuration for the outdoor channel model shown in Figure 13

The results obtained from the outdoor channel simulation states that the distance between transmitter and receiver is 151.95m, and that at that distance, the received signal power is -89.29dBm. Considering that the transmitted signal power is 30dBm, the path losses are the difference of the signal power between the transmitter and the receiver, 119.29dB.

For the indoor channel model, the obtained results are shown in Figure 15. Similarly with the outdoor channel model, two points can be noticed, one red, which represents the transmitter location, and another one green, which represents the receiver location.

The configuration for this simulation is shown in the Figure 16; 10GHz carrier frequency, transmission power reduced to 0.01W, or 10dBm, and 1 m grid resolution. The losses introduced here for the indoor and outdoor walls, and the ground are 6dB, 4dB, and 9dB, respectively.

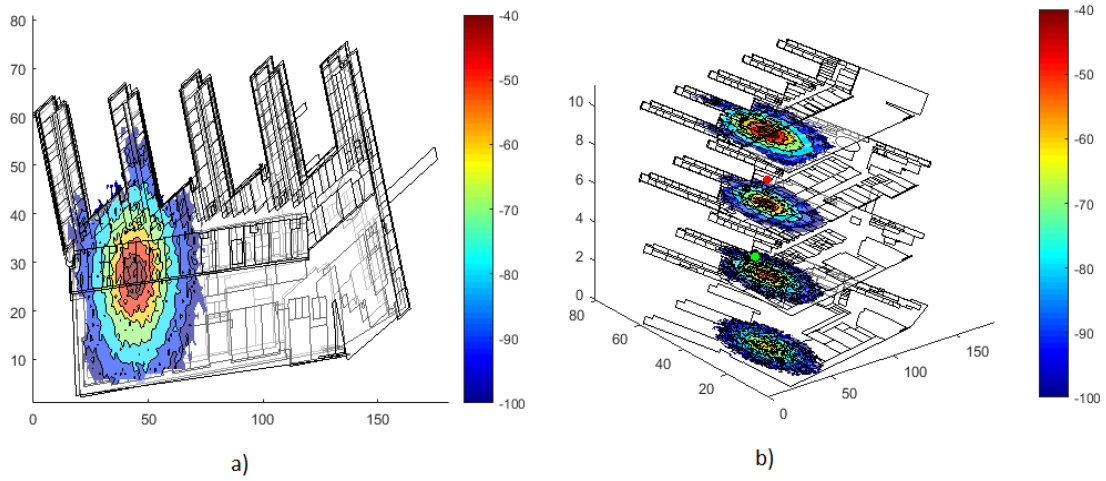

Figure 15. a) Indoor channel model power map in 2D; b) Indoor channel model power map in 3D

The obtained results for this configuration and this scenario are that for a distance of 39.05m between the transmitter and the receiver, the received power level is -74.72dBm. Considering the 10dBm of transmitted power, the losses are 84.72dB. From this 84.72dB, 56.4dB are due to the path loss, 6dB due to the ground, 8dB caused by the indoor or room walls, and the rest, 14.32dB caused by the shadowing.

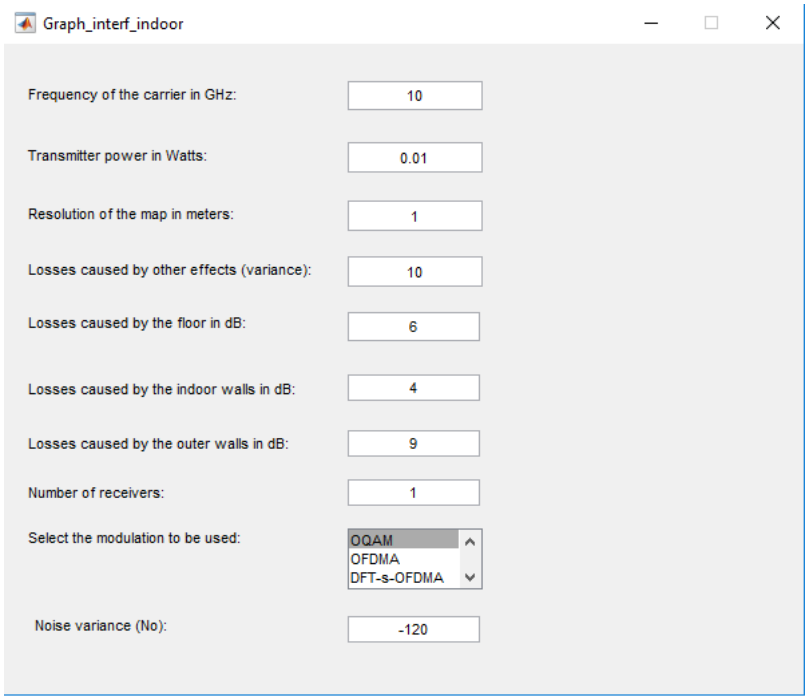

Figure 16: Network configuration for the indoor channel model shown in Figure 14

8.2 Positioning estimation error

For the positioning estimation, two different types of simulations have been implemented: one with increasing SNR values and fixed distance, and a second one with fixed SNR and increasing distance. To perform all these simulations, 50 independent data realizations have been used.

The main objective of the first simulation was to understand the behavior of the three considered 5G waveforms for low, medium, and high SNR values. This way it will be possible to check which waveform has a better performance at low SNR values. These simulation-based results will be then checked with the CRLB computations.

In Figure 17, it is possible to analyze the behavior of the CRLB for the implemented distance estimator. In Figure 17 a), the range of SNR values (from -16dB to 26dB), is shown and the CRLB value related to each SNR value for the three waveforms. In Figure 17 b) a zoomed look is given for low SNR values also for the three waveforms.

From the CRLB point of view, the CP-OFDMA waveform has a slightly better accuracy than the other two. This is shown in the Figure 17.

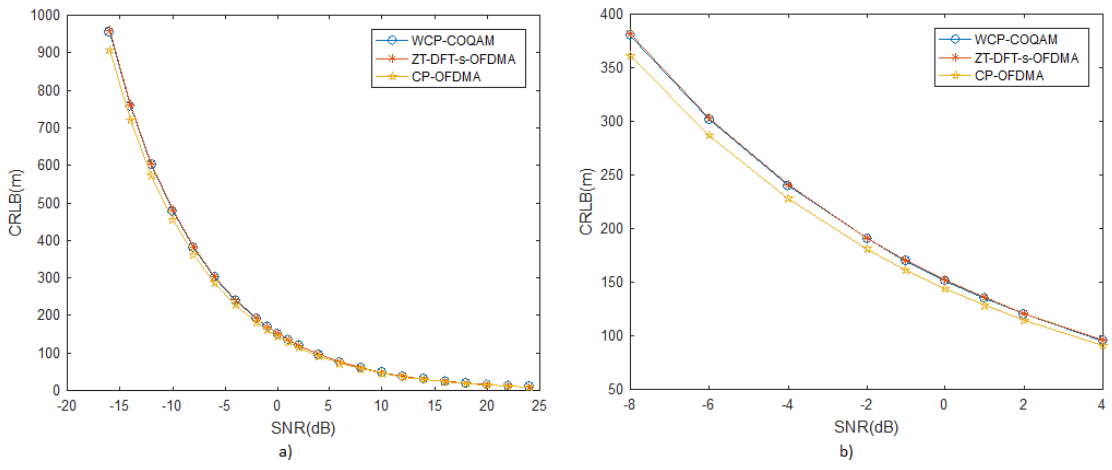

Figure 17. a) CRLB for a wide range of SNR values for the three waveforms b) zoomed look of the CRLB in a small range of SNR values

With the second simulation, the performance of the different waveforms for different distances between the transmitter and the receiver was analyzed. For that, the estimated distance is computed based on the correlation between the incoming signal and a reference OFDM waveform. The results are shown in Figure 18. Several modulation orders, from 4-QAM till 64-QAM, were used in conjunction with the 5G OFDM waveforms.

As it is shown in the Figure 18, there is no influence of the user modulation order on the performance of the distance estimation. For the same 5G waveform, the same result has been achieved independently on the QAM modulation order that was used.

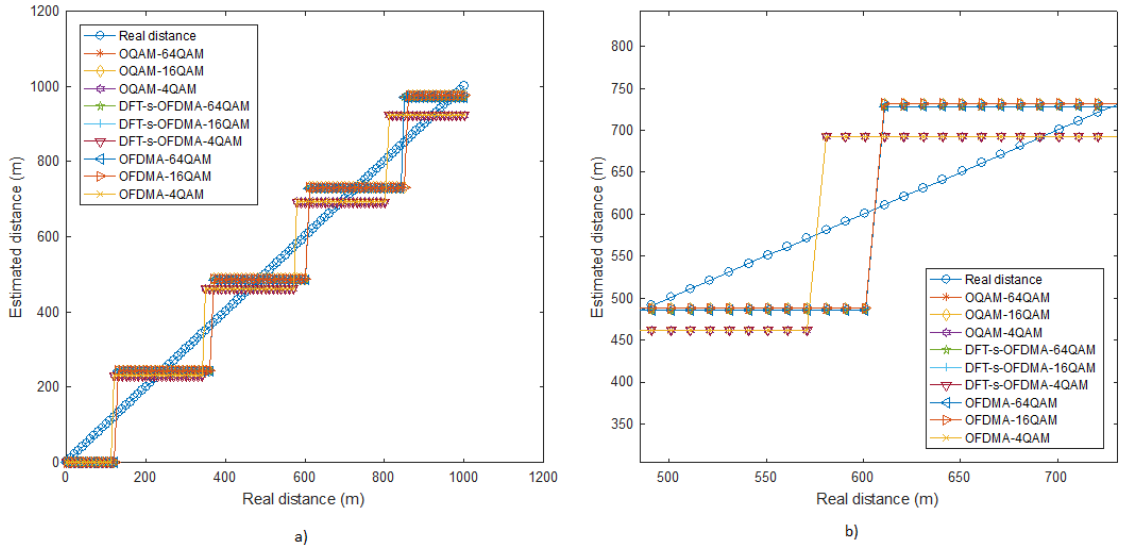

Figure 18. a) estimated distance for a wide range of real distances values for the three waveforms and different modulations; b) zoomed look of the estimated distance in a small range of real distance values.

Analyzing the Figure 18 closely, it seems that the waveform CP-OFDMA has the best accuracy of the three waveforms, as concluded also from the Figure 17. To have it clearer, the distance error as a function of the real distance is shown in Figure 19.This time, as it was previously concluded that the modulation order has no influence in the distance estimation, only the results relative to the modulation 4QAM are shown.

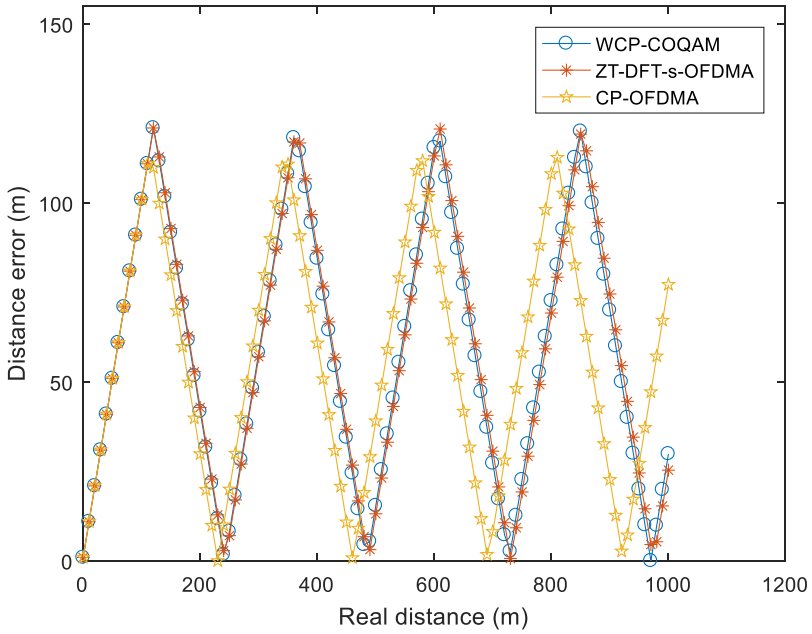

Figure 19. Distance error for the 3 different waveforms as a function of the distance between the access node and the mobile terminal.

The values plotted in Figure 19 show the mean values computed over the 50 iterations. The obtained results show the distance error obtained after the distance estimation. Considering that for the working sampling frequency, 1.25MHz, the distance accuracy is about 120m, and this is the maximum values of the distance error obtained in Figure 19. So, if the distance between the transmitter and the receiver is below to the mentioned 120m (the accuracy), the output of the autocorrelation function will be a delay of 0 samples, and thus, the distance estimation will be 0m. Once the distance is bigger than 120m, the transmitter will have 1 sample of delay, which is translated in a distance estimation of approximately 240m, making the distance error decrease.

The obtained results confirm that CP-OFDMA is slightly outperforming the other two considered 5G waveforms, but that the differences in performance are very small. The mean values for the distance estimation error are 58.95m, 59.36m, and 56.1m for the WCP-COQAM, ZT-DFT-s-OFDMA, and CP-OFDMA, respectively. As the differences are of the order of cm for an error of the order of tens of meters, one could conclude that there is no significant difference between the three considered 5G waveforms in terms of positioning accuracy.

8.3 QoS in communications

For the quality of service part, the performance of the different waveforms was analyzed. BER was selected as the comparative performance criterion. The results are shown in Figure 20,Figure 21, and Figure 22, for three QAM modulation orders, namely 4, 16, and 64, respectively.

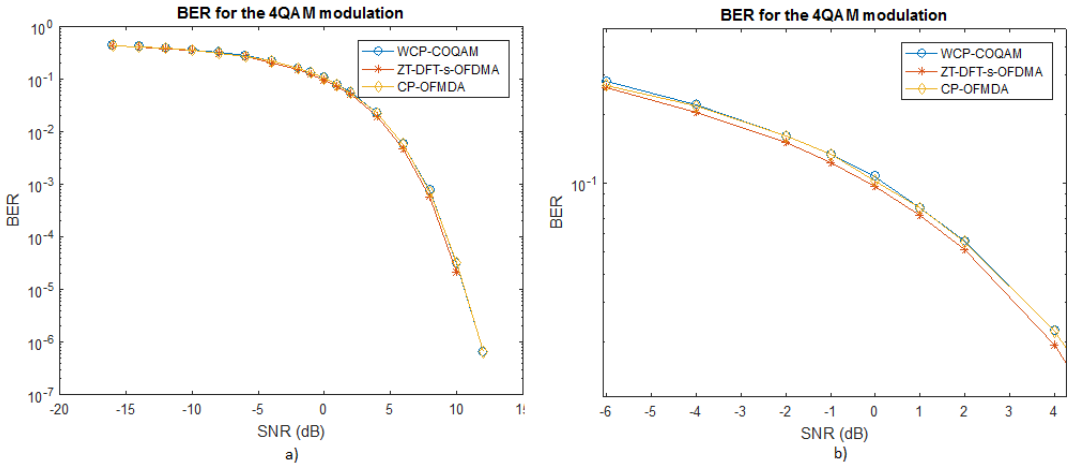

Figure 20. :a) BER for a wide range of SNR values for the three waveforms with modulation 4QAM; b) zoomed look of the BER in a small range of SNR values

From the results in Figure 20, Figure 21, and Figure 22, the conclusion that can be taken is that, from the point of view of the QoS of a communication system, the ZT-DFT-s-OFDMA is slightly outperforming the other two, but again the differences are not significant

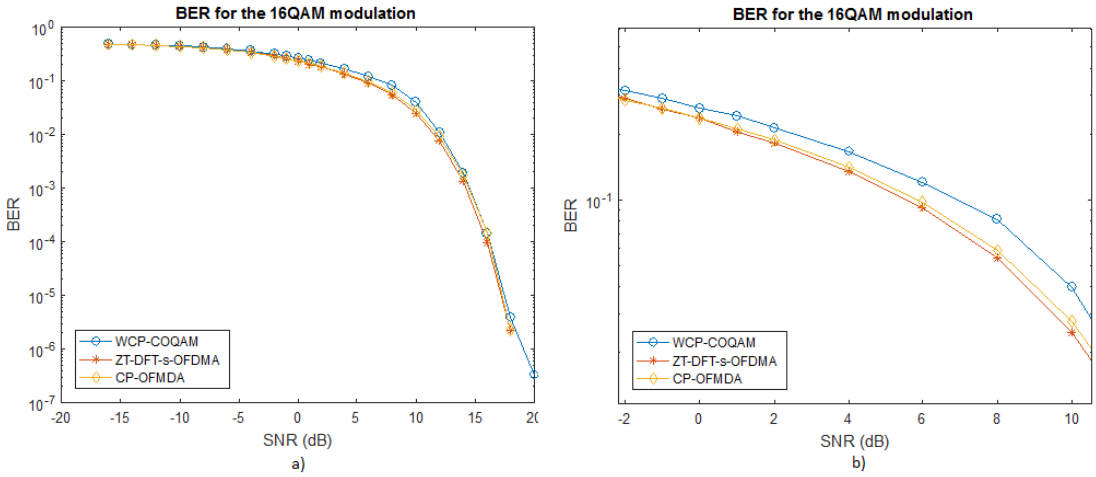

Figure 21. a) BER for a wide range of SNR values for the three waveforms with modulation 16QAM; b) zoomed look of the BER in a small range of SNR values

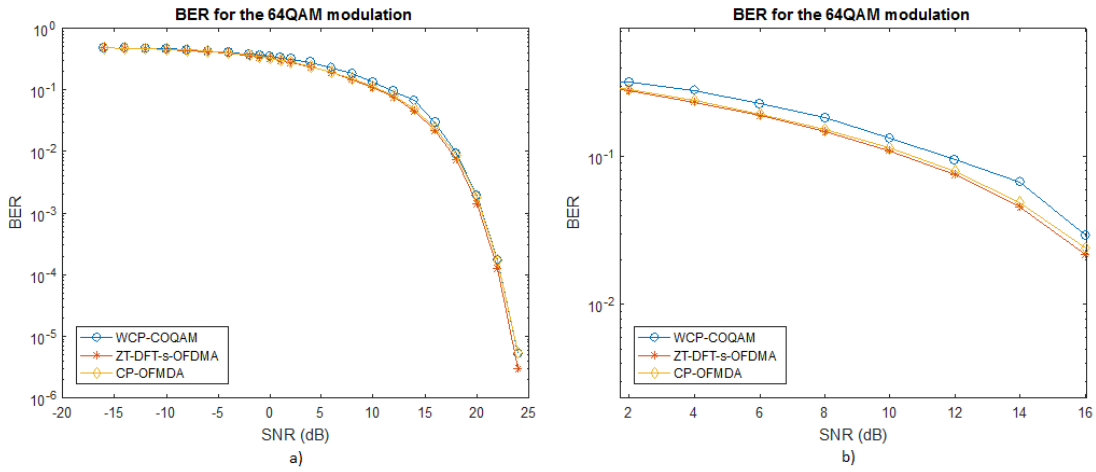

Figure 22. a) BER for a wide range of SNR values for the three waveforms with modulation 64QAM; b) zoomed look of the BER in a small range of SNR values

The difference between the use of different modulation orders is that, a higher SNR is needed to reach the same QoS requirement. This is shown in Figure 23, where the QoS of the system is shown for the different modulation orders and SNR values.

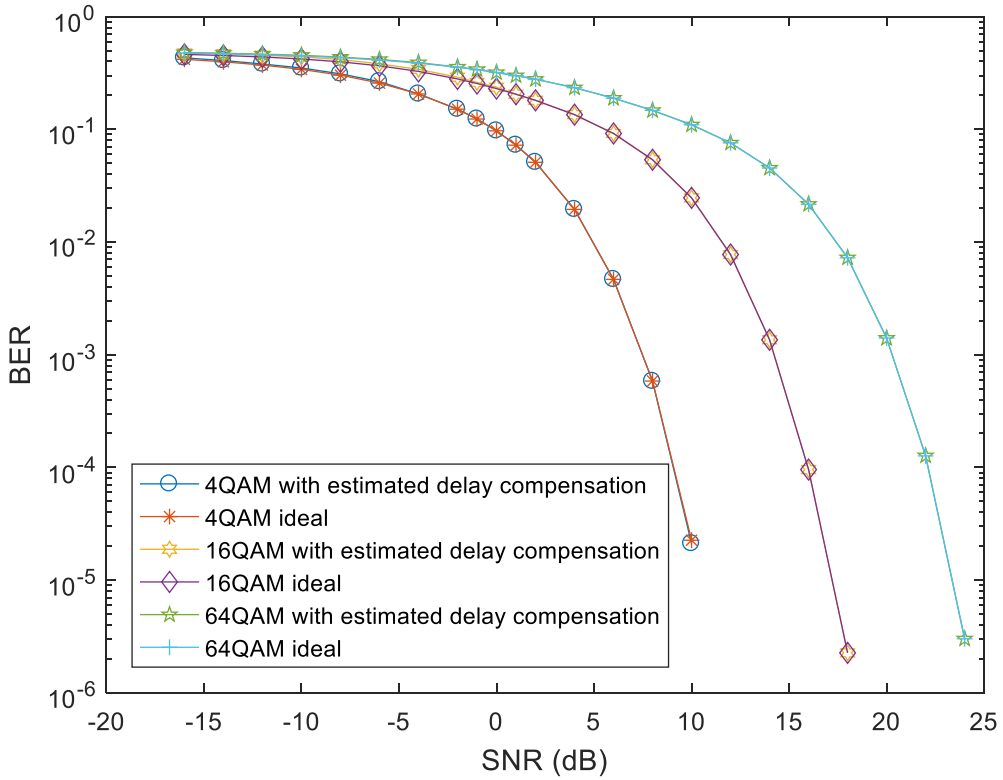

Figure 23: BER performance for different modulation orders for ZT-DFT-s-OFDMA

From the Figure 23 it can be concluded that in order to achieve the same BER performance, the higher the modulation order, the higher the required SNR level. For example, to obtain the same performance with 16QAM, about 7dB higher SNR is required in

comparison with the 4QAM modulation and about 15dB higher SNR is needed in the case of the 64QAM compared to 4QAM. This can be also analyzed with the other two waveforms, whose results are shown in the Figure 24 and Figure 25 for CP-OFDMA and WCP-COQAM, respectively.

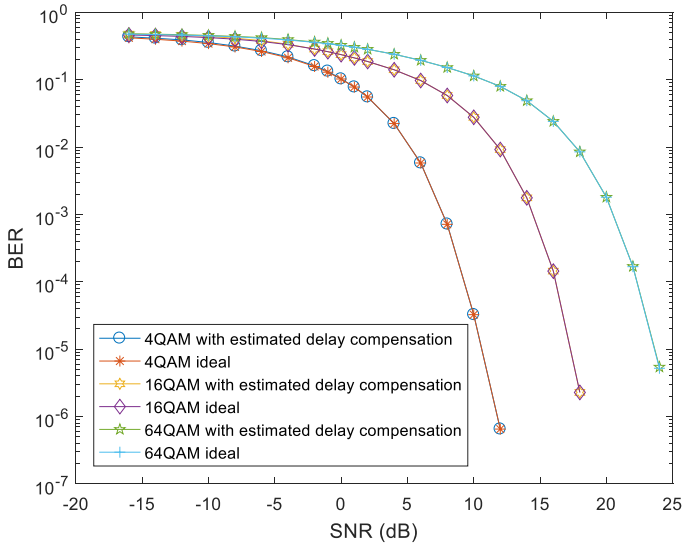

Figure 24: BER performance for different modulation orders for the CP-OFDMA

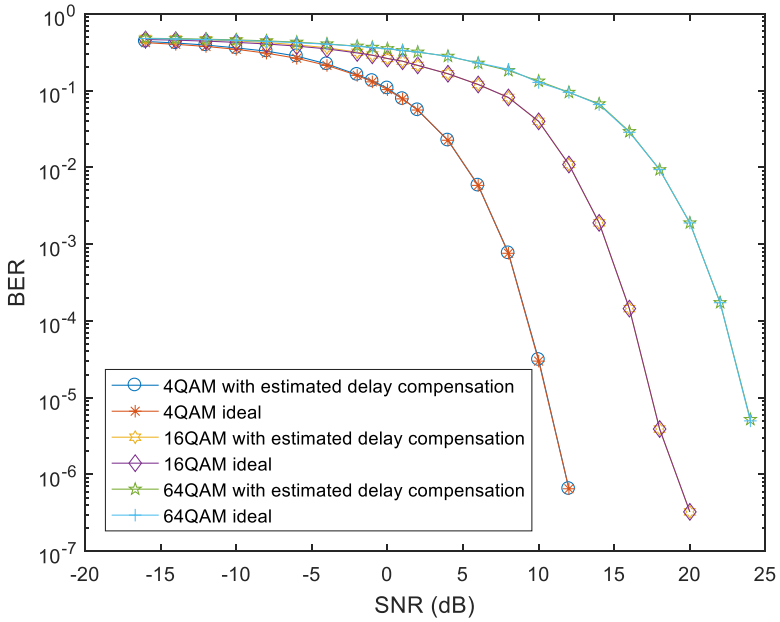

Figure 25: BER performance for different modulation orders for the WCP-COQAM

9. CONCLUSIONS

In this thesis, we addressed the issue of joint communication and positioning waveforms in 5G communications. Three different waveforms where considered, namely WCP-COQAM, ZT-DFT-s-OFDMA, and CP-OFDMA. In order to evaluate the positioning and communication targets, two channel models have been defined and implemented, one for outdoor scenarios, which is based on the channel model developed on the European METIS project, and another one for the indoor scenarios, based on the single-tap channel model and TUT building maps.

With this simulation tool, the coverage areas have been studied, by visualizing with the help of a power map the RSS values of each point of the maps. For this purpose, the positions of the transmitter and the receiver have been randomly selected. The considered channel included the channel LOS delay, the path loss effects and AWGN. Future studies are dedicated to include multipath fading effects in each of these two channels.

With the implemented channel, the positioning and communication performance of the three 5G waveforms was studied. The chosen performance criteria have been the positioning accuracy, expressed through distance-estimation error and CRLB of the distance estimate, and the communication QoS, expressed through BER curves.

The results obtained from these simulations, show that the modulation order used has no influence in the distance estimation. With the different QAM modulations, similar results were obtained. Regarding the 5G waveform choice, we have also seen that there are only minor differences between the three considered waveforms both in terms of positioning and communication. CP-OFDMA is slightly more accurate than the other two in terms of positioning performance, while the waveform with slightly better performance than the other two in terms of communication performance at low SNR values is ZT-DFT-s-OFDMA. The obtained values here are also rather similar, with a difference of 1dB from one waveform to another to obtain the same BER value. In terms of communication, the change in the achievable BER with different QAM modulation orders is significant, with a difference of about 7dB of SNR between the 4QAM and 16QAM, and around 15dB between the values obtained with 4QAM and 64QAM.

To implement the transmission, an oversampling factor of 50 has been used, in order to be able to increase the sampling frequency of the transmitting signal from 25.08 kHz to 1.25MHz. The oversampling should be higher in order to obtain more accurate distance estimation, however due to very long simulation times and insufficient computing resources, we have not studied in details the scenarios with more than 50 oversampling

factor. For example, with an oversampling factor 6000, more than one week of simulations are needed for a reliable statistical result.

As mentioned in the section 6.4, the oversampled should be of around 6000 to reach to the sampling frequency that is desired to reach 153.6 MHz according to the [57]. With sampling rate, the accuracy will be reduced to 1.95m. Increasing the number of samples transmitted, the lower the sample duration, the bigger the number of samples sent, and thus, more accurate will be the position estimation.

For future implementations, the oversampling factor can be increased to 400 or even more in order to obtain more suitable results. In addition, new 5G waveforms can be implemented, checking if the obtained results are still so close from one waveform to another. Also, it is possible to add new metrics to the measurements, such as, power efficiency or the data capacity.

Regarding to the channel models, as it has been mentioned, the biggest problem in the position estimation is when the multipath occur. This can be analyzed in future projects, by implementing some of the solutions reported in the literature, such as the one shown in [54].

Another way of extending the results achieved in this thesis is to implement a complete TOA system, i.e., to implement at least four transmitters in order to have the user position and not only the distance estimation between the transmitter and the receiver. Processing the signals of the, at least, four transmitters the positioning accuracy will be improved. There is also the possibility of adding an AOA system in order to improve also the position accuracy.

10. REFERENCES

[1] A. Lee Swindlehurst, G. Seco-Granados, “OFDM pilot optimization for the communication and localization trade-off”, 2010.

[2] https://www.metis2020.com/. The METIS web page

[3] 3GPP webpage. Available: http://www.3gpp.org/technologies/keywords-acronyms/99-hspa

[4] 5G Forum Service Sub-committee, “5G new wave towards future societies in the 2020S”, 2015 5G White Paper, http://www.5gforum.org/#!untitled/c7bg, 2015

[5] “5G: A technology vision”, Huawei White Paper, 2013. [Online]. Available: http://www.huawei.com/5gwhitepaper/

[6] White paper “NGMN 5G white paper”, NGMN Alliance, https://www.ngmn.org/uploads/media/NGMN_5G_White_Paper_V1_0.pdf

[7] El Hattachi, R. et al., “NGMN 5G initiative white paper”, NGMN Alliance working paper, 2014. https://www.ngmn.org/uploads/media/141222_NGMN-Executive_Version_of_the_5G_White_Paper_v1_0.pdf

[8] “Making 5G NR a reality”, Qualcomm Technologies Inc., September 2016. Available: https://www.qualcomm.com/documents/making-5g-nr-reality

[9] T. Rappaport, S. Sun, R. Mayzus, H. Zhao, Y. Azar, K.Wang, G. Wong, J. Schulz, M. Samimi, and F. Gutierrez, “Millimeter wave mobile communications for 5G cellular: It will work!” IEEE Access, vol. 1, pp.335-349,2013.

[10] P. Zhouyue and F. Khan, “An introduction to millimeter-wave mobile broadband systems,” IEEE Communications Magazine, vol. 49, no. 6, pp. 101-107, 2011.

[11] Md. Maruf Ahamed and S. Faruque, “Propagation factors affecting the performance of 5G millimeter wave radio channel”.

[12] F. Schaich and T. Wild, “Waveform contenders for 5G – OFDM vs. FBC vs. UFMC”, Special Session on Signal Processing Techniques for Future Mobile Networks @ 6th Int.l Symposium on Communications Control and Signal Processing (ISCCSP), April 2014.

[13] U. Kumar, C. Ibars, A. Bhorkhar, “A waveform for 5G: guard interval DFT-s-OFDMA”, IEEE Globecom International Workshop on Emerging Technologies for 5G Wireless Cellular Networks, 2015.

[14] G. Berardinelli et al., “On the potential of zero-tail DFT-spread-OFDM in 5G networks”, Proc. IEEE Veh. Tech. Conf., pp.1-5, May 2014.

[15] “5G waveform & multiple access techniques”, Qualcomm, November 4, 2015.

[16] X. Cui, T.A. Gulliver, J. Li and H. Zhang, “Vehicle positioning using 5G millimeter-wave systems”, Special Section ON Green Communications and Networking for 5G Wireless, November 2016.

[17] M. Farooq, M.I. Ahmed and U.M. Al, “Future generations of mobile communication networks”, Academy of Contemporary Research Journal, January 2013.

[18] R. Khutey, G. Rana, V. Dewangan, A. Tiwari and A. Dewamngan, “Future of wireless technology 6G & 7G”, International Journal of Electrical and Electronics Research, June 2015.

[19] R. S. Campos, “Evolution of positioning techniques in cellular networks, from 2G to 4G”, Wireless Communications and Mobile Computing Volume 2017, 2017 https://www.hindawi.com/journals/wcmc/2017/2315036/

[20] A. De Groote, “GSM positioning control”, Mobile Business Seminar, January 2005.

[21] S. Sand, A. Dammann, and C. Mensing, *Positioning in Wireless Communication Systems*. Germany, 2014

[22] P. Brida, P. Cepel, J. Duha, “The accuracy of RSS based positioning in GSM networks”, *Proc. Of 16th International Conference of Microwaves Radar and Wireless Communications-MIKON 2006*, vol. 2, pp. 541-544, 2006, ISBN 83-906662-7-8.

[23] M. Hate, “Empirical formula for propagation loss in land mobile radio services”, *IEEE Trans. veh.Tech.*, vol 29, pp. 317-325, Aug. 1980.

[24] Y. Zhao, “Standardization of mobile phone positioning for 3G systems”, IEEE Communications Magazine, 40(7): 108-116, July 2002

[25] A. Brachs et al., “A novel radio multiservice adaptive network architecture for 5G networks”, *Vehicular Technology Conference (VTC Spring) 2015 IEEE 81 st*, pp 1-5, 2015

[26] S. Fischer, “Observerd time difference of arrival (OTDOA) positioning in 3GPP LTE”, Qualcomm Technologies, Jun. 2014.

[27] “Requirements and KPIs for 5G mobile and wireless system”, METIS deliverable D1.1, 2013. Available: https://www.metis2020.com/wp-content/uploads/deliverables/METIS_D1.1_v1.pdf

[28] K. Hamdi, “On the statistics of signal-to-interference plus noise ratio in wireless communications”, *IEEE Trans. Commun.*, vol. 57, no. 11, pp. 3199-3204, Nov. 2009

[29] X. Ge, J. Ye, Y. Yang, Q. Li, “User mobility evaluation for 5G small cell networks based on individual mobility model”, *IEEE Journal on Selected Areas in Communications*, vol. 34, no. 3, pp. 528-541, March 2016

[30] S. Yunas, M. Valkama, J. Niemelä, “Spectral and energy efficiency of ultra-dense networks under different deployment strategies”, *IEEE Commun. Mag.*, vol. 53, no. 1, pp. 90-100, Jan. 2015

[31] Z. Chaloupka, “Technology and standardization gaps for high accuracy positioning in 5G”, *IEEE Communications Standards Mag.*, vol 1, no. 1, pp. 59-65, Mar. 2017

[32] F.M. Dahunsi, B. Dwolatzky, “Statistical Analysis of the Accuracy of Location Measurements Provided for LBS in South Africa”, AFRICON, 2011, pp. 1-5, 2011, ISSN 2153-0033

[33] R.Filjar, L. Bušić, S. Dešić, D. Huljenić, “LBS position estimation by adaptive selection of positioning sensors based on requested QoS”, in *Lecture notes in computer science*, Vol. 5174, S. Balandin, D. Moltchanov, Y. Koucheryavy; Ed. Berlin: International Conference on Next Generation Wired/Wireless Networking, 2008, pp. 101-109

[34] I. K. Adusei, K. Kyamakya, K. Jobmann, “Mobile positioning technologies in cellular networks: an evaluation of their performance metrics”, *Proc. MILCOM 2002*, vol. 2, pp. 1239-1244, Oct. 2002

[35] Y. Sun, Z. Zhou, S. Tang, X. K. Ding, J. Yin, Q. Wan, “3D Hybrid TOA-AOA Source Localization using an Active and a Passive Station”, *2016 IEEE 13th International Conference on Signal Processing (ICSP)*, pp. 257-260, 2016, ISBN 978-1-5090-1345-6

[36] 3GPP TS 22.071 V 8.0.0, “3rd Generation Partnership Project; technical specification group services and system aspect; location services (LCS); Service description; Stage 1” (Release 8).

[37] A. Dammann, T. Jost, R. Raulefs, M. Walter, S. Zhang, “Optimizing Waveforms for Positioning in 5G”, *2016 IEEE 17th International Workshop on Signal Processing Advances in Wireless Communications (SPAWC)*, 2016, ISBN 978-1-5090-1749-2

[38] Z. Abu-Shaban, X. Zhou, T. Abhayapala, G. Seco-Granados, H. Wymeersch, “Error bounds for uplink and downlink 3D localization in 5G mmWave systems”, Available: https://arxiv.org/pdf/1704.03234.pdf

[39] A. Hakkarainen, J. Werner, M. Costa, K. Leppänen, M. Valkama, “High-efficiency device localization in 5G ultra-dense networks: prospects and enabling technologies”, *Proc. IEEE (VTC Fall)*, pp. 1-5, Sep. 2015

[40] J. Werner, J. Wang, A. Hakkarainen, D. Cabric, M. Valkama, “Performance and Cramer-Rao bounds for DoA/RSS estimation and transmitter localization using sectorized antennas”, *IEEE Trans. Veh. Technol.*, vol. 65, no. 5, pp. 3255-3270, May 2016

[41] A. D. Angelis, C. Fischione, “Mobile Node Localization via Pareto Optimization: Algorithm and Fundamental Performance Limitations”, *IEEE Journal on Selected Areas in Communications*, vol. 33, no. 7, pp. 1288-1303, 2015.

[42] S. Fischer, H. Koorapaty, E. Larsson, A. Kangas, “System performance evaluations of mobile positioning methods”, *Proc. IEEE 49th Vehicular Technology Conf. (VTC) 1999*, vol. 3, pp.1962-1966, 1999

[43] J. James, J. Caffery, L.S. Gordon, “Overview of Radiolocation in CDMA Cellular Systems”, *IEEE Communications Magazine*, vol. 36, pp.38-45, April 1998.

[44] F. M. Dahunsi, B. Dwolatzky, “Conceptual Framework that Supports Environment-Aware Positioning and Improved QoS for Location Based Services”, *Proc. 9th IEEE African Conference Nairobi (AFRICON ’09)*, pp. 1-6, 23-25 Sep. 2009

[45] R. Exel, T. Sauter, “A comparison of time- and RSS-based radio localization for the factory floor”, *Proc. IEEE Workshop Factory Communication Systems*, pp. 13-20, May 2012

[46] Li Li, J.L. Krolik, “Simultaneous Target and Multipath Positioning”, *IEEE Journal of Selected Topics in Signal Processing*, vol. 8, no. 1, pp. 153-165, Feb. 2014

[47] D. Dardari, A. Conti, U. Ferner, A. Giorgetti, M. Z. Win, “Ranging with ultrawide bandwidth signals in multipath environments”, *Proceedings of the IEEE*, vol. 97, no. 2, pp. 404-426, Feb. 2009

[48] K. Witrisal et al., “High-accuracy localization for assisted living: 5G systems will turn multipath channels from foe to friend”, *IEEE Signal Process. Mag.*, vol. 33, no. 2, pp. 59-70, Mar. 2016.

[49] M. Ulmschneider, R. Raulefs, C. Gentner, M. Walter, “Multipath assisted positioning in vehicular applications”, *2016 13th Workshop on Positioning, Navigation and Communications (WPNC),* pp. 1-6, 2016, ISBN 978-1-5090-5440-4.

[50] K. Witrisal, P. Meissner, “Performance bounds for multipath-assisted indoor navigation and tracking (MINT)”, *IEEE International Conference in Communications (ICC),* Ottawa, Canada, 2012.

[51] J. Werner, M. Costa, A. Hakkarainen, K. Leppanen, M. Valkama, “Joint user node positioning and clock offset estimation in 5G ultra-dense network”, *Proc. IEEE Global Communications Conference (GLOBECOM),* Dec. 2015.

[52] H. Lin, P- Siohan, “Multi-carrier modulation analysis and WCP-COQAM proposal”, *EURASIP Journal on Advances in Signal Processing,* Dec. 2014.

[53] METIS, “D1.4 channel models,” February 2015.

[54] J.A. del Peral-Rosado, “Evaluation of the LTE Positioning Capabilities in Realistic Navigation Channels”, Ph.D. Dissertation, 2014.

[55] A. Shahmansoori, R. Montalban, J. A. Lopez-Salcedo, G. Seco-Granados, “Design of OFDM Sequences for joint communications and positioning based on the asymptotic expected CRB”, *Int. Conf. Localization and GNSS,* Jun. 2014.

[56] F. Burkhardt, E. Eberlein, S. Jaeckel, G. Sommerkorn, R. Prieto-Cerdeira, “MIMOSA-a dual approach to detailed land mobile satellite channel modeling”, *International Journal of Satellite Communications and Networking,* vol. 32, no. 4, Jul. 2014.

[57] T. Eichler, “5G Technology Introduction, Market Status Overview and Worldwide Trials”, *5G & IoT Seminar (IST) Lisbon,* 2014 [online]. Available: http://grow.tecnico.ulisboa.pt/wp-content/uploads/2014/03/5G-StandardizationMarketPHY_TaroEichler.pdf

[58] A. Shahmansoori, R. Montalban, G. Seco-Granados, “Effect of Channel Variability on Pilot Design for Joint Communications and Positioning in OFDM”, *2014 11th International Symposium on Wireless Communications Systems (ISWCS),* pp. 292-296, 2014, ISBN 978-1-4799-5863-4.

[59] A. Shahmansoori, R. Montalban, J. A. Lopez-Salcedo, G. Seco-Granados, “Design of OFDM sequences for joint communications and positioning based on the asymptotic expected CRB”, *Int. Conf. Localization and GNSS*, Jun. 2014.

[60] J. Zheng, Y.-C. Wu, “Joint time synchronization and localization for an unknown node in wireless sensor networks”, *IEEE Trans. Signal Process.*, vol. 58, no. 3, pp. 1309-1320, Mar. 2010.

[61] H. Zhou, Y.-F. Huang, “A maximum likelihood fine timing estimation for wireless OFDM systems”, *IEEE Trans. Broadcasting*, vol. 52, no. 2, pp.159-164, Jun. 2004.

[62] D. Wubben, P. Rost, J.S. Bartelt, M. Lalam, V. Savin, M. Gorgoglione, A. Dekorsy, G. Fettweis, “Benefits and Impact of Cloud Computing on 5G Signal Processing: Flexible centralization through cloud-RAN”, *IEEE Signal Processing Magazine*, vol. 31, no. 6, pp. 35-44, 2014.

[63] P. Rost, C. J. Bernardos, A. De Domenico, M. Di Girolamo, M. Lalam, A. Maeder, D. Sabella, D. Wübben, “Cloud technologies for flexible 5G radio access networks”, *IEEE Communications Magazine,* vol. 52, no. 5, pp. 68-76, May 2014.

[64] A. Imran, A. Zoha, “Challenges in 5G: how to empower SON with big data for enabling 5G”, *IEEE Network*, vol. 28, no. 6, pp. 27-33, 2014.

[65] K. Zheng, “Big data-driven optimization for mobile networks toward 5G”, *IEEE Network*, vol. 30, no. 1, pp. 44-51, Jan. 2016.

[66] M. R. Bhalla, A. V. Bhalla, “Generations of Mobile Wireless Technology: A Survey”, *International Journal of Computer Applications*, vol. 5, no.4, Aug. 2010.

[67] S. Shukla, V. Khare, S. Garg, P. Sharma, “Comparative study of 1G, 2G, 3G and 4G”, *Journal of Engineering, Computers & Applied Sciences (JEC&AS)*, vol. 2, no.4, Apr. 2013.

[68] P. Bode, A. Lampe, M. Helfenstein, “Combined GSMK and 8PSK modulation for GSM and EDGE”, *Proc. IEEE Int. Symp- Circuits Syst. (ISCAS)*, PP- 614-617, 2013.

[69] P. Guan, D. Wu, T. Tian, J. Zhou, X. Zhang, L. Gu, A. Benjebbour, M. Iwabuchi, Y. Kishiyama, “5G field trials – OFDM-based waveforms and mixed numerologies”, *IEEE Journal on Selected Areas in Communications*, Mar. 2017.

[70] Z. Wang, S. Fan, Y. Rui, “CDMA-FMT: A novel multiple access scheme for 5G wireless communications”, *2014 19th International Conference on Digital Signal Processing (DSP)*, Aug. 2014, ISBN 978-1-4799-4612-9.

[71] X. Yu, T. Wild, F. Schaich, “Impact of RF transmitter hardware on 5G waveforms: Signal conditioning for UF-OFDM”, *2016 International Symposium on Wireless Communication Systems (ISWCS),* 2016, ISBN 978-1-5090-2061-4.

[72] H. Cho, Y. Yan, G.-K. Chang, X. Ma, “Asynchronous Multi-User Uplink Transmission for 5G with UFMC Waveform”, *2017 IEEE Wireless Communications and Networking Conference (WCNC),* 2017, ISBN 978-1-5090-4183-1.

[73] G. R. Al-Juboori, A. Doufexi, A. R. Nix, “System level 5G evaluation of GFDM waveforms in an LTE-A platform”, *2016 International Symposium on Wireless Communication Systems (ISWCS),* 2016, ISBN 978-1-5090-2062-1.

[74] D. Porcino, “Performance of a OTDOA-IPDL positioning receiver for 3G – FDD mode”, *Proc. of IEEE 3G Mobile Communication Technologies Conference,* pp. 221-225, 2001.

[75] H. Yan, D. Cabria, “Compressive sensing based initial beamforming training for massive MIMO millimetre-wave systems”, *IEEE Global Conference on Signal and Information Processing (GlobalSIP),* pp. 620-624, 2016.

[76] M. Koivisto, M. Costa, A. Hakkarainen, K. Leppänen, M. Valkama, “Joint 3D positioning and network synchronization in 5G ultra-dense networks using UKF and EKF”, Aug. 2016. [Online], available: http://arxiv.org/abs/1608.03710

[77] Z. Chunmei, O. Jikun, Y. Yunbin, “Positioning accuracy and reliability of GALILEO, integrated GPS-GALILEO system based on single positioning model”, *Chinese Science Bulletin,* vol. 50, bi. 12, pp. 1252-1260, 2015.

[78] O. Delgado, F. Labeau, “Delay aware load balancing over multipath wireless networks”, *IEEE Transaction on Vehicular Technology,* Jan. 2017.

[79] C. Gentile, N. Alsindi, R. Raulefs, C. Toelis, “Geolocation Techniques: Principles and Applications”, 2013.

[80] A. A. Adebomehin, S. D. Walker, “Enhanced Ultrawideband LOS Sufficiency Positioning and Mitigation for Cognitive 5G Wireless Setting”, *2016 39th International Conference on Telecommunications and Signal Processing (TSP),* pp. 87-93, 2016.

[81] K. Ratajczk, K. Bakowski, K. Wesolowski, “Two-way relaying for 5G systems: Comparison of network coding and MIMO techniques”, *2014 IEEE Wireless Communications and Networking Conference (WCNC),* pp.376-381, 2014

[82] R.-A. Pitaval, B. M. Popović, M. Mohammad, R. Nilsson, J. J. van de Beek, “Spectrally-Precoded OFDM for 5G wideband operation in fragmented sub-6GHz

Spectrum", 2016. [Online], Available: https://arxiv.org/ftp/arxiv/papers/1606/1606.00623.pdf

[83] T. S. Rappaport, S. Sun, M. Shafi, "5G channel model with improved accuracy and efficiency in mmWave bands", *IEEE 5G Tech Focus*, vol. 1, no. 1, Mar. 2017.

[84] J. Medbo, P. Kyosti, K. Kusume, L. Raschkowski, K. Haneda, T. Jamsa, V. Nurmela, A. Roivainen, J. Meinila, "Radio propagation modelling for 5G mobile and wireless communications", *IEEE Communications Magazine*, vol. 54, no. 6, pp. 144-151, Jun. 2016.

[85] S. Gault, W. Hachem, P. Ciblat, "Joint sampling clock offset and channel estimation for OFDM signals: Cramer-rao bound and algorithms", *IEEE Transactions on Signal Processing*, vol. 54, no. 5, pp. 1875-1885, May 2006.

[86] L. Sanguinetti, M. Morelli, "An initial ranging scheme for IEEE 802.16 based OFDMA systems", *2011 8th International Workshop on Multi-Carrier System & Solutions (MC-SS)*, 2011.

[87] J. Medbo, K. Börner, K. Haneda, V. Hovinen, T. Imai, J. Järvelainen, T. Jämsä, A. Karttunen, K. Kusume, J. Kyröläinen, P. Kyösti, J. Meinilä, V. Nurmela, L. Raschkowski, A. Roivainen, J. Ylitalo, "Channel modelling for the fifth generation mobile communications", *2014 8th European Conference on Antennas and Propagation (EuCAP)*, pp. 219-223, 2014.

[88] H. Lin, P. Siohan, "Multi-carrier modulation analysis and WCP-COQAM proposal", *EURASIP Journal on Advances in Signal Processing*, Nov. 2014.

[89] S. R. Schnur, "Identification and classification of OFDM based signals using preamble correlation and cyclostationary feature extraction", Ph.D. Thesis dissertation, 2009.